ABSTRACT

Effect of Oncomodulin on Afferent Inner Hair Cell and Efferent Outer Hair Cell Synaptopathy

Pierce Thompson

Director: Dwayne Simmons, Ph.D.

Inner hair cells (IHCs) are a type of specialized sensory cell which converts the pressure gradient of the endolymph into an interpretable signal, allowing for hearing. However, there is another type of sensory cell crucial for hearing: outer hair cells (OHCs). OHCs amplify basilar membrane motion through the movement of prestin, a voltage-sensitive motor protein, resonating with its respective tonotopic frequency. The medial olivocochlear (MOC) system is part of the auditory system which synapses on OHCs with cholinergic receptors, acting antagonistically to prestin by hyperpolarizing the cell, resulting in cochlear acoustic protection through a calcium dependent mechanism. Loss of function of the MOC system has been shown to precede progression of age-related sensory deficits, but the correlation between the loss of function of the MOC system and OHC vitality is yet to be examined. This paper will examine the correlation between OHC vitality, efferent MOC synapses, and afferent glutaminergic synapses.

APPROVED BY DIRECTOR OF HONORS THESIS:

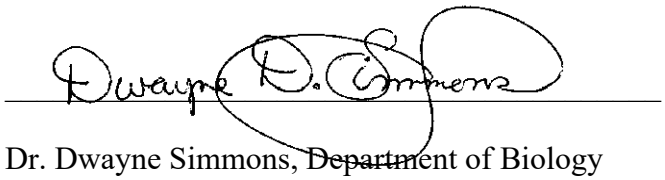

Dr. Dwayne Simmons, Department of Biology

APPROVED BY THE HONORS PROGRAM:

_____

Dr. Elizabeth Corey, Director

DATE: _____

EFFECT OF ONCOMODULIN ON AFFERENT INNER HAIR CELL AND EFFERENT OUTER HAIR CELL SYNAPTOPATHY

A Thesis Submitted to the Faculty of

Baylor University

In Partial Fulfillment of the Requirements for the

Honors Program

By

Pierce Thompson

Waco, Texas

May 2022

TABLE OF CONTENTS:

LIST OF FIGURES

LIST OF TABLES

ACKNOWLEDGEMENTS

I would like to thank my thesis mentor Dr. Dwayne Simmons for the opportunity to carry out this project, other members of Simmons Lab for their help and advice, and my parents for supporting and encouraging me to finish this project. Additionally, I want to thank the Folmar Research Fund for their financial support in this project.

CHAPTER ONE:

INTRODUCTION

1.1 Statement of Purpose

The effect of the medial olivocochlear system in providing efferent synaptic feedback to outer hair cells to protect from acoustic trauma is essential to hearing functionality (Boero et al. 2018). However, how this system, and its degradation, effect afferent synaptic transmission remains unknown.

The purpose of this thesis project is to act as a pilot study examining the role of the medial olivocochlear system in protecting hearing. The efferent signaling of the medial olivocochlear system is thought to have a protective effect on OHC vitality, among other functions (Boero et al. 2018). This study examines the number of afferent synapses, efferent synapses, and OHC counts in aging mice, showing a method in which these synapses can be identified, classified, and counted. By comparing these groups, the protective effect of these efferent synapses can be shown by its correlative effect on IHC synaptopathy, as well as OHC vitality. Additionally, the use of oncomodulin knock-out (KO) mice show an accelerated age-related hearing loss phenotype that can further show the effects of synaptopathy.

1.2 Sensorineural Hearing Loss

According to the World Health Organization, currently over five percent of the world's population has a disabling form of hearing loss, requiring rehabilitation. Furthermore, it is projected that by the year 2050, one in ten people will have 'disabling'

hearing loss- that is, hearing loss greater than 35 dB in one or both ears. It is estimated that one billion young adults are at risk of permanent, avoidable hearing loss caused by noise induced hearing loss (NIHL) as a result of unsafe listening practices. Both NIHL and age-related hearing loss (presbycusis) can occur as a result of damage to the nerve pathways connecting the hair cells to the brain. Recent research suggests that this type of neural degeneration, cochlear synaptopathy, is what causes hidden hearing loss (HHL) (Kujawa and Liberman 2009). HHL is a type of hearing loss characterized by a temporary hearing threshold shift following acoustic exposure where the hair cells recover, but the spiral ganglia neurons do not (Kujawa and Liberman 2009). A threshold shift can be observed when, for example, one has increased difficulty hearing after a loud event, such as a concert. The HHL model suggests that while normal hearing function returns as the hair cells recover, the neurons do not. It has been proposed that the medial olivocochlear efferent system plays a crucial role in preventing HHL and synaptopathy in various studies (Boero et al. 2018). Therefore, a greater understanding of this system, and how it impacts and interacts with hearing, is crucial.

1.3 Inner Ear Anatomy

The ear is composed of three parts: the outer, middle, and inner ear, the latter of which will be the focus of this paper. The outer ear is the easily visible external portion of the ear and functions to collect sound pressure from the area of the pinna and transfer it to the tympanic membrane (Pickles 1988). The middle ear consists of three ossicles, the malleus, the incus, and the stapes. These bones transfer the pressure that arrives at the tympanic membrane to the oval window, a component of the inner ear. The inner ear has a semicircular component, a vestibular component, and a cochlear component. Figure 1

displays the anatomy of these three parts. The semicircular component contains three semicircular canals in the X, Y, and Z planes and detects angular acceleration using the cristae in the ampullated ends of each canal. The vestibular component contains the utricle and saccule (Pickles 1988). The maculae and otoliths within the utricle and saccule detect linear acceleration, as well as horizontal and vertical head rotation respectively (Pickles 1988).

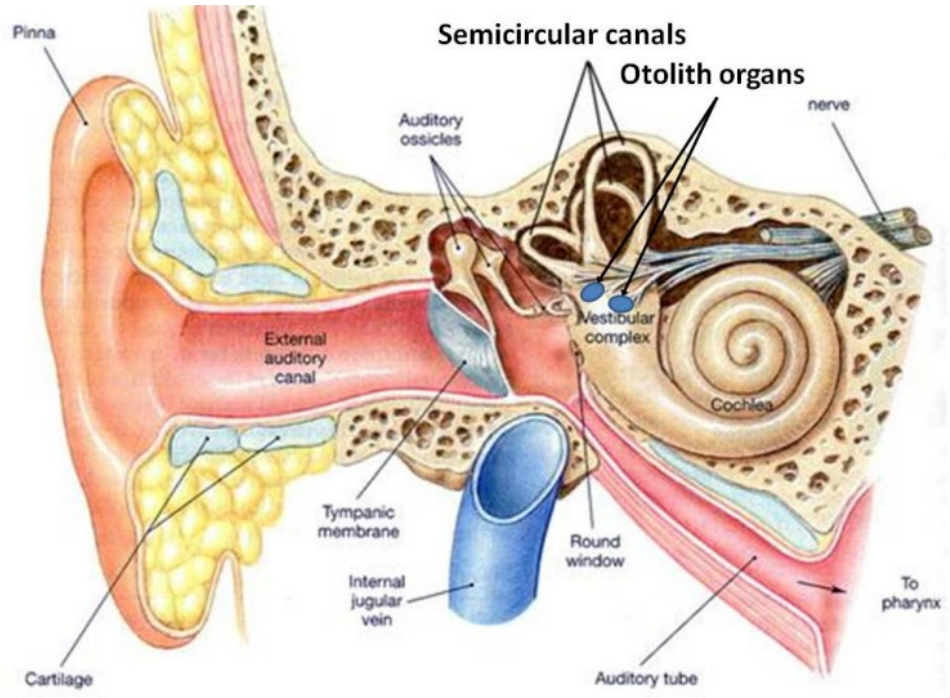

Figure 1: Diagram of the outer, middle, and inner ear (Martini 1998)

The cochlea is a snail-shell shaped sensory organ which converts the pressure gradient delivered from the ossicles at the oval window into an electrochemical signal which the brain can interpret as sound. Figure 2 shows an unwound version of the cochlea, better illustrating how sound waves travel through the cochlea. Within the cochlea are three fluid filled tubes which carry sound waves to hair cells, the sensory cells of hearing. Sound waves, now converted to a pressure wave within the fluid, first travels through the scala vestibuli until it reaches the apex of the cochlea, the helicotrema (Pickles 1988). The pressure wave then travels through the scala tympani until it terminates at the round window which is found in the middle ear, allowing for pressure equalization via the eustachian tube. The scala vestibuli and scala tympani are filled with perilymph, a solution with high sodium concentration (138 mM), low potassium concentration, (6.9 mM), and a resulting voltage of -70 mV (Bosher and Warren 1968).

The scala vestibuli and scala tympani flow above and below the cochlear duct. The cochlear duct is physically separated from the scala vestibuli and scala tympani by Reissner's membrane and basilar membrane, respectively. The scala media (cochlear duct) is filled with endolymph, a solution with high potassium concentration (154 mM), low sodium concentration (91 mM), and a resulting voltage of +80 mV, contrary to perilymph (Bosher and Warren 1968).

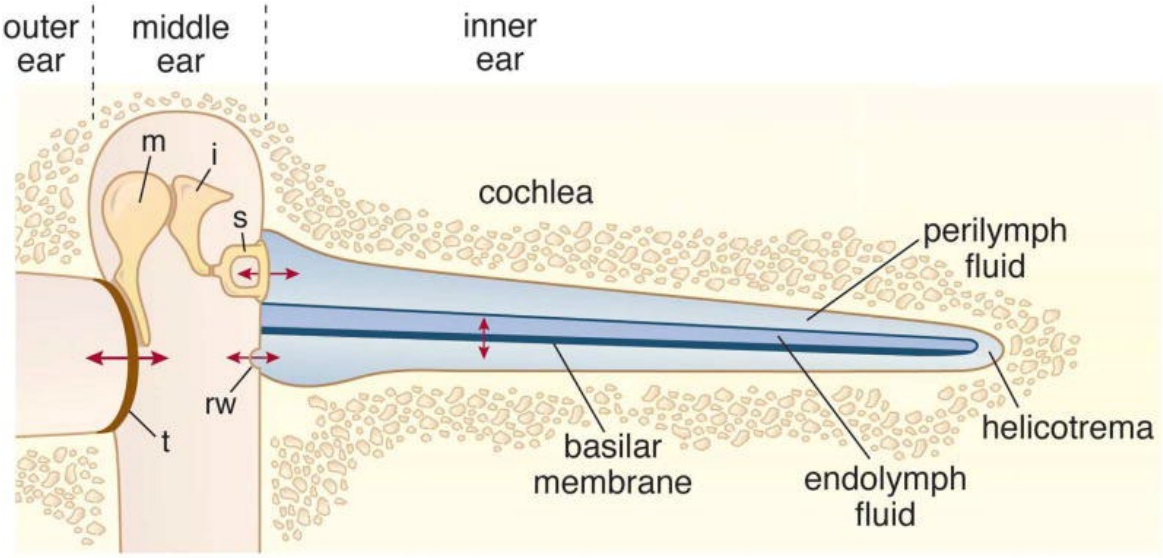

Figure 2: Simplified model of a cochlea; note the cochlear duct spirals upward in a snail-shell shape in typical mammalian populations. rw = round window, m = malleus, i = incus, s = stapes, t = tympanic membrane (Fettiplace 2017)

The solute concentrations of the endolymph are maintained by the stria vascularis, a type of specialized, stratified epithelium found along the lateral wall of the cochlear duct shown in Figure 3 (Pickles 1988). The difference in solute concentrations and subsequent voltage between perilymph and endolymph creates an electrochemical gradient which hair cells use for signaling purposes.

1.3 Basilar Membrane

The cochlear duct contains several components critical for proper hearing functionality, most of which are shown in Figure 3. Of these, the basilar membrane is perhaps one of the most important, as it contains the hair cells which allow for sound to be interpreted. As the basilar membrane travels up towards the apex of the cochlea it gets thicker and more motile, resulting in different parts of the basilar membrane resonating with different frequencies of sound (P Dallos, Popper, and Fay 1996). Therefore, the

cochlea is considered tonotopic. High frequency sounds resonate best where the basilar membrane is thin and stiff, while low frequency sounds resonate best where it is thick and easily motile. As a result, the apical cochlea responds to low frequency sound, while the basilar cochlea responds to high frequency sound. Basilar membrane characteristics determine where a sound's *characteristic frequency* is, or, where the basilar membrane best resonates with it (Müller et al. 2005).

The organ of Corti rests on top of the basilar membrane across its length throughout the cochlear duct. The features of the organ of Corti include the inner and outer hair cells, the tectorial membrane, and other structural and supporting cells. The inner and outer hair cells are the sensory cells of the inner ear and will be discussed in depth later. The tectorial membrane is a gelatinous membrane that contacts the stereocilia of inner and outer hair cells to elicit an action potential (Ghaffari, Aranyosi, and Freeman 2007). In a cross-sectional view of the organ of Corti it is revealed that there is typically three OHCs resting upon three Deiter cells, two pillar cells which separate the more medial IHCs from the more lateral OHCs, one IHC resting upon two inner phalangeal cells, and inner sulcus cells medial to the IHCs (Fettiplace 2017). A layer of connective tissue is found in the organ of Corti, made from inner phalangeal cells, pillar cells, Deiter cells, and the apical tips of IHCs and OHCs (Fettiplace 2017). The tight junctions found in this connective tissue create a barrier that keeps the endolymph chemically separate from the perilymph of the scala tympani, a crucial function for the maintenance of the electrochemical gradient used in auditory signaling (Nadol et al. 1976). A similar barrier, Reissner's membrane, is found above the tectorial membrane, separating the endolymph from the perilymph of the scala vestibuli.

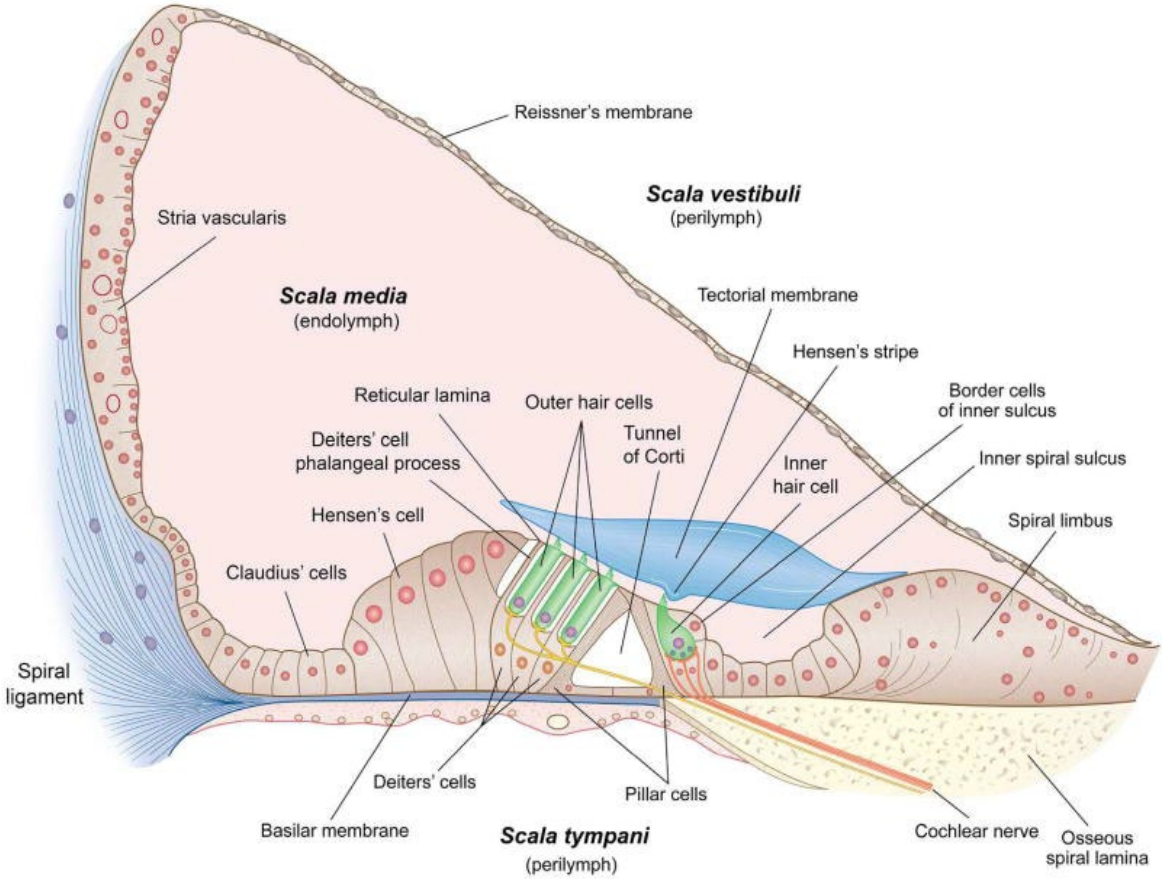

Figure 3: Cross-section of the organ of Corti (Fettiplace 2017)

1.4 Hair Cell Anatomy and Physiology

The organ of Corti contains two types of hair cells: the more medial IHCs, and the more lateral OHCs. Both OHCs and IHCs have microvilli on their apical ends which insert into the cuticular plate (terminal web), an area of the apical hair cell dense with actin filaments in which the microvilli are anchored, as shown in Figure 4 (Pollock and McDermott Jr 2015). Hair cell microvilli are referred to as stereocilia and have a stair-step pattern going from shortest to tallest stereocilia. When sound causes the basilar membrane to resonate, the stereocilia of IHCs deflect either in the direction of the kinocilium as they brush against the tectorial membrane, depolarizing the cell (positive

deflection), or they deflect away from the tallest stereocilia, and the cell becomes hyperpolarized (negative deflection) (P Dallos, Popper, and Fay 1996). The taller stereocilia are connected to the shorter stereocilia via cadherin-23 tip links, and protocadherin-15, which ensures that when the tallest stereocilia is deflected in either direction, the other stereocilia also deflect (Fettiplace 2017). Deflection of the stereocilia opens various mechanoelectrical transduction (MET) ion channels. These mechanically gated ion channels are connected to protocadherin-15 of tip links, and thus open or close depending on the positive or negative deflection of the stereocilia, allowing for nonspecific cations from the endolymph (mainly K+, Na+, and Ca2+) to enter the cells (Qiu and Müller 2018). Following the influx of mainly K+ (because of endolymph composition), voltage gated calcium channels (VGCC) of the IHC will open, further depolarizing the cell and allowing for vesicle fusion to occur at the basilar end of the hair cell and thus afferent synaptic transmission to occur through the release of the neurotransmitter glutamate (Corns et al. 2018). The signal then propagates down type I afferent auditory nerve fibers to the ventral cochlear nucleus, eventually terminating at the auditory cortex. OHCs can also transmit sound through type II afferent auditory nerve fibers, though these are unmyelinated and only compose about 5% of the total afferent auditory nerve fibers (Carricondo and Romero-Gómez 2019).

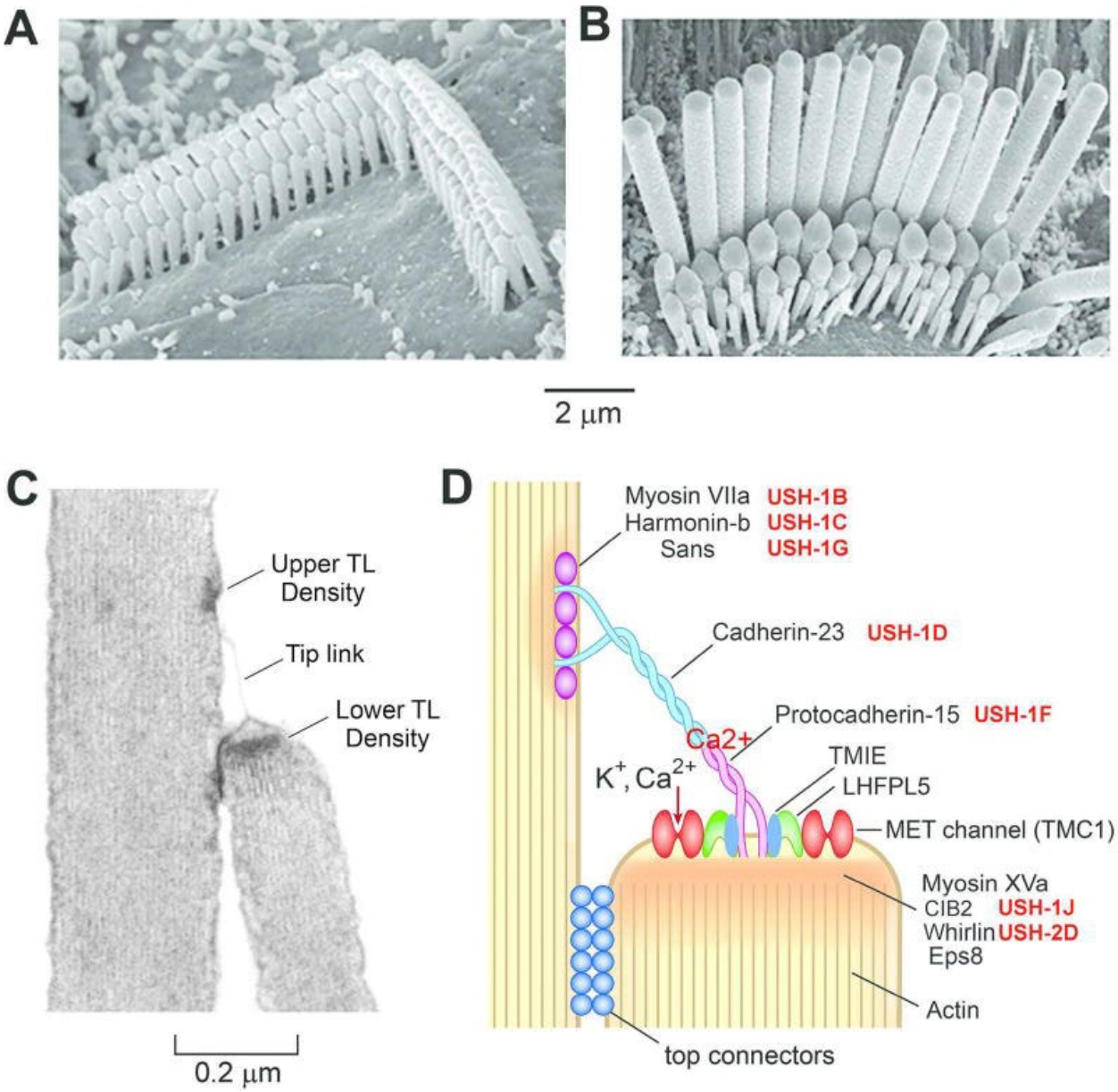

Figure 4: SEM images of (A) OHC stereocilia, and (B) IHC stereocilia. (C) TEM image of OHC tip link connecting two stereocilia. (D) Diagram of tip link protein composition (Fettiplace 2017)

OHCs use the same mechanism as IHCs for activation via stereocilium mechanics and MET channel opening. Following K+ influx, VGCCs open, resulting in an increase of intracellular ionic calcium. This depolarizes the OHC and results in prestin, a voltage sensitive motor protein, contraction (M. Charles Liberman et al. 2002). In piezoelectric

devices, mechanical stress, as opposed to an external voltage, causes charge separation and subsequent capacitance. For example, when the lattice structure of quartz crystals is subjected to mechanical stress at a specific angle, there is a resulting charge separation and thus electric potential created. Biological piezoelectricity is used in OHCs to actuate cellular expansion or contraction (depending on the hyperpolarized or depolarized state of the cell, respectively) via prestin, facilitating cellular electromotility (Liu and Neely 2009). As the lateral membrane bound prestin expands and contracts in response to a change in voltage, so too does the OHC expand or contract. As such, the electromotive characteristics of prestin are directly tied to cochlear amplification capabilities of OHCs. The stereocilia of OHCs are thought to be connected to the tectorial membrane, while the stereocilia of IHCs are not (P Dallos, Popper, and Fay 1996). Because of this, when OHCs contract, they bring the tectorial membrane closer to the stereocilia of IHCs, allowing for easier activation and processing of sound. Prestin of OHCs has an electromotility half-activation close to the resting membrane potential of OHCs at -45 to -55 mV, allowing for optimal cellular contraction and expansion (Fettiplace 2017). Therefore, when OHCs are hyperpolarized, prestin relaxes and elongates, making the OHC elongate, physically separating the IHCs from the tectorial membrane, decreasing the ability of IHCs to detect sound.

1.5 Neuroanatomy and Physiology

Following hair cell depolarization via positive direction stereocilia deflection, IHCs transfer the action potential to afferent synapses where they are ultimately transferred to and interpreted by the brain. As the stereocilia deflect, MET channels open, allowing for the potassium ions of the endolymph to enter and depolarize the cell. The

resulting change in voltage opens VGCCs, such as Cav1.3 (Johnson and Marcotti 2008). The resulting change in intracellular calcium concentration allows for vesicle fusion at the basal portion of the cell. The synaptic ribbon protein, CtBP2, increases the surface area that neurotransmitter-containing vesicles can anchor to, allowing for more robust and sustained transmission to occur (Buran et al. 2010). The neurotransmitter glutamate, released from these vesicles, then binds to GluA2 (also called GluR2 for glutamate receptor 2) which initiates the action potential which will propagate up the nervous system to the brain.

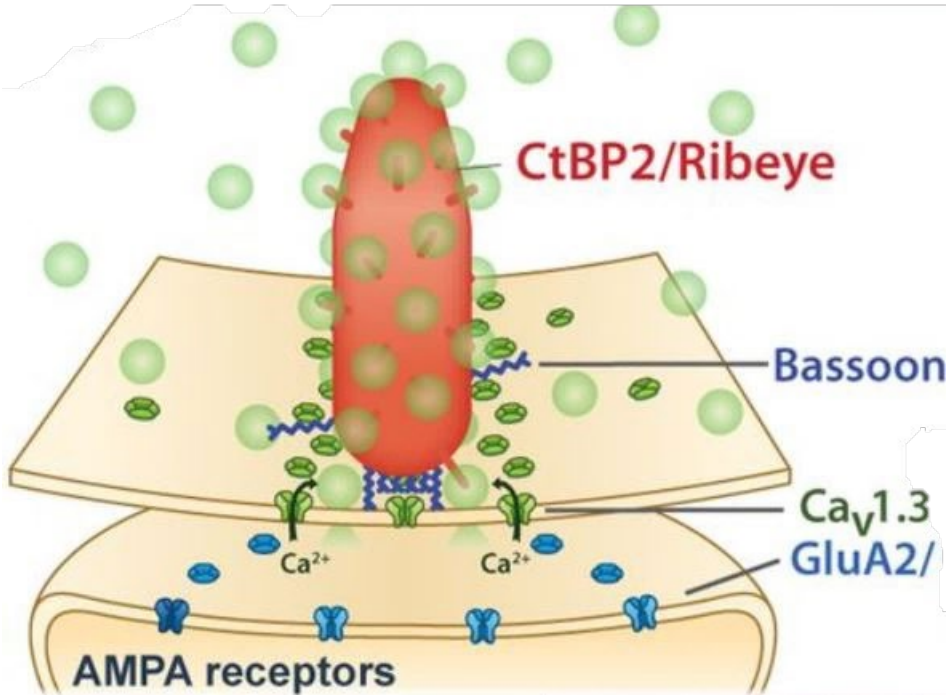

Figure 5: Afferent synaptic terminal of IHC (above) and type 1 afferent dendrite (below) with relevant proteins and ion movement shown (Jing et al. 2013)

Typically, when discussing hearing, only afferent, ascending pathways are discussed as they are how sensory input is received. However, efferent, descending pathways are also crucial in understanding how sensory input is received by the brain as

they have the capacity to modulate the information that is relayed into the auditory cortex (Pickles 1988). In this way hearing is not composed of strictly static decibel thresholds, but rather, dynamic ones. One such efferent innervation is received by the cochlea from the superior olivary complex (SOC). The SOC contains several subnuclei: the lateral superior olive, the medial superior olive, the medial nucleus of the trapezoid body, and various other pre-olivary and peri-olivary nuclei (Pickles 1988). Efferents of the olivocochlear (OC) system are divided into medial and lateral groups, depending on the respective origin of their parental cell bodies in the SOC, as well as their site of termination (Warr and Guinan 1979). Medial olivocochlear (MOC) efferents originate in the medial superior olivary nuclei and synapse directly onto OHCs, while lateral olivocochlear (LOC) efferents originate in the lateral superior olivary nuclei and synapse onto the dendrites of type I afferent auditory nerve fibers (Lopez-Poveda 2018). MOC and LOC efferents can be categorized into crossed and uncrossed fibers, which correlates to which cochlea, the contralateral or ipsilateral cochlea, the efferents terminate onto (Rasmussen 1946). The majority of MOC fibers are crossed, terminating on the contralateral cochlea, while the majority of LOC fibers are uncrossed, terminating on the ipsilateral cochlea (P Dallos, Popper, and Fay 1996). MOC fibers are cholinergic, meaning that they make use of the neurotransmitter acetylcholine, and myelinated, meaning they are coated in a myelin sheath which insulates and boosts the electrical signal within the axon (S. F. Maison et al. 2012). LOC fibers do not interact with OHCs, are hard to stimulate electrically due to their unmyelinated nature, and their function tends to be species specific (M. C. Liberman and Brown 1986). As such, there is little consensus on their functionality, and therefore they will not be the focus of this paper.

1.6 MOC efferent function

The ipsilateral MOC efferent reflex is when sound from one ear activates the MOC reflex to protect that same ear. This involves crossed efferents; the MOC efferents project to and subsequently from the ventral nucleus of the trapezoid body (VNTB) of the contralateral side of the brain; however, the axons cross the midline of the brain twice in this process, resulting in ipsilateral suppression (Lopez-Poveda 2018). The contralateral MOC efferent reflex uses uncrossed efferents to traverse the midline of the brain to reach the VNTB, then it remains on that side, traveling to the contralateral ear to carry out its suppressive effect (Lopez-Poveda 2018). Figure 6 diagrams these neuronal pathways for sake of understanding.

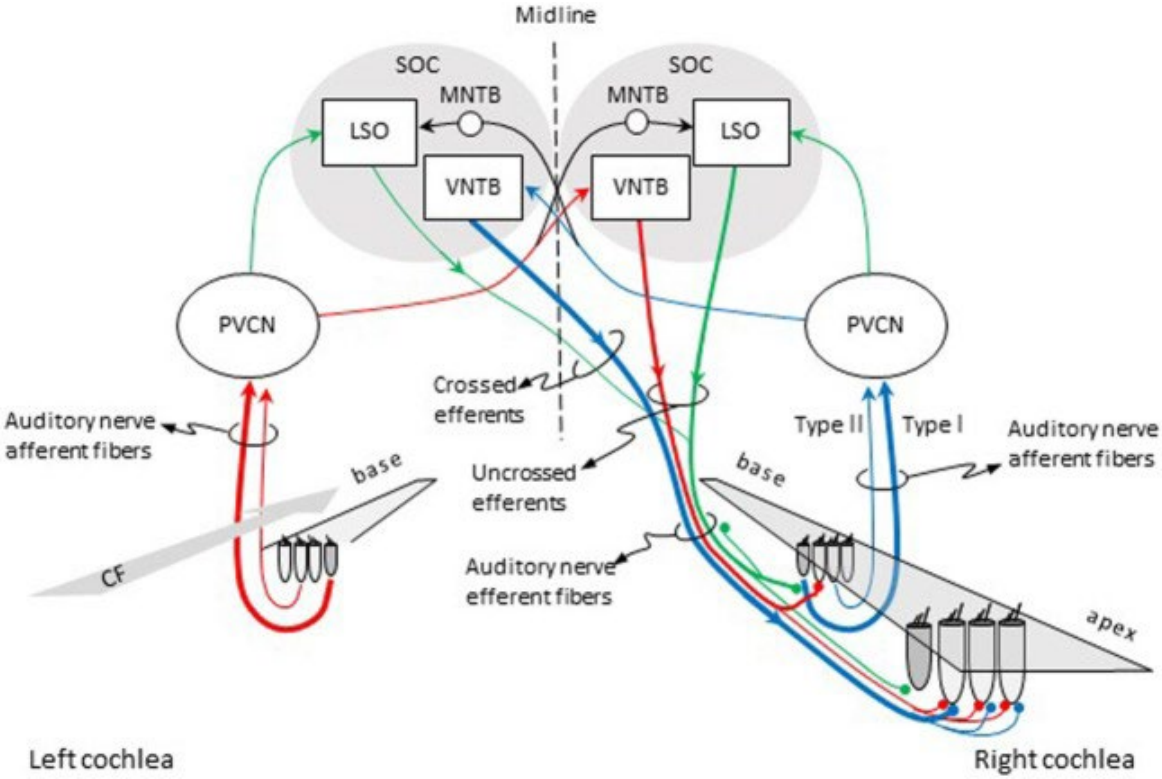

Figure 6: Medial and lateral olivocochlear efferent neuron pathways. Red lines represent contralateral MOC reflex. Blue lines represent ipsilateral MOC reflex. Green lines show LOC reflex. SOC = Superior Olivary Complex. LSO = Lateral Superior Olive. PVCN = Postero-Ventral Cochlear Nucleus (Lopez-Poveda 2018)

Where the MOC efferent reflex activation begins is a contentious issue. The predominant theory is that the reflex begins with activation of the auditory nerve through type I afferent activation (on IHCs) (Brown, de Venecia, and Guinan 2003). However, some research shows that mutant mice lacking type II afferents (on OHCs) have no MOC efferent response, though it has been contended that this mutant line had a loss of efferent transmission rather than a loss of sensory drive (Froud et al. 2015; S. Maison, Liberman, and Liberman 2016).

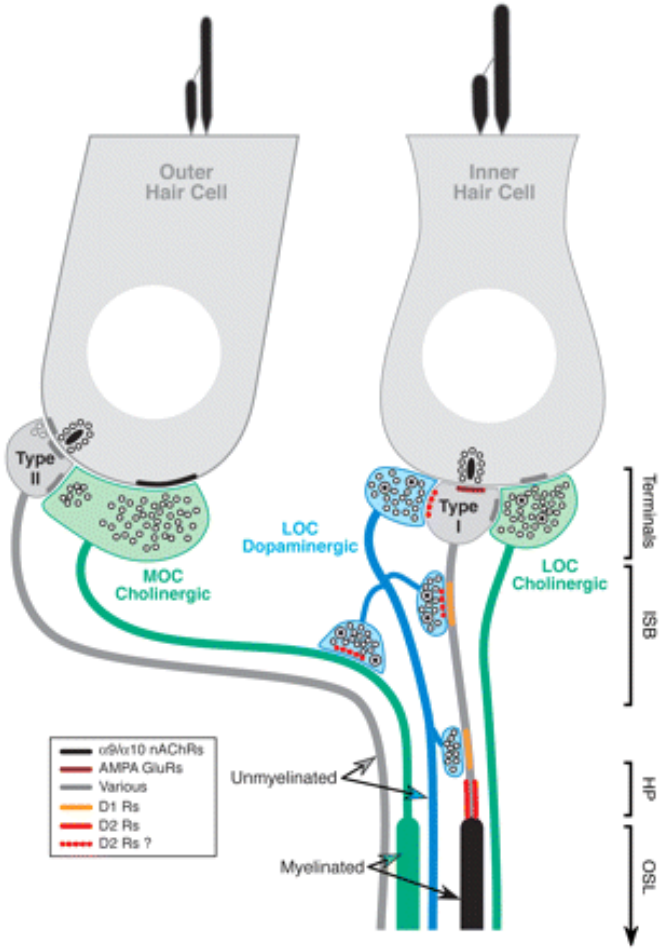

Figure 7: Synaptic terminals of IHCs and OHCs (Maison et al. 2012)

MOC efferent synapses terminate basally on OHCs, as is shown in Figure 7. The neurotransmitter acetylcholine is released into the synaptic cleft upon activation, activating α9α10 nicotinic cholinergic receptors (nAChR) to uptake calcium ions. These calcium ions then activate coupled calcium-activated potassium ion channels, causing the OHC to release potassium ions, hyperpolarizing the cell. Pharmacological studies show that this potassium ion channel belongs to the small conductance calcium ion activated SK family, more specifically, of SK2 nature. SK2 is a heteromeric complex of SK-α subunits and calmodulin, an EF-hand calcium binding protein which acts as a calcium sensor and signal transducer, shown in Figure 8. SK2 responds to changes in intracellular calcium ion concentrations in a voltage-independent manner. The coupled function of nAChR and SK2 as an inhibitory postsynaptic current (IPSC) is further evidenced by the complete inhibition of IPSCs through application of strychnine or dequalinium, respective nAChR and SK2 specific inhibitors (Gifford and Guinan 1987). Additionally, various studies have shown evidence of a possible calcium-induced-calcium-release through ryanodine receptor expression on synaptoplasmic cisterna which act as calcium reserves, resulting in greater activation of SK2 channels following calcium uptake from nAChR activation, allowing for a greater number of SK2 channels to be activated (Lioudyno 2004).

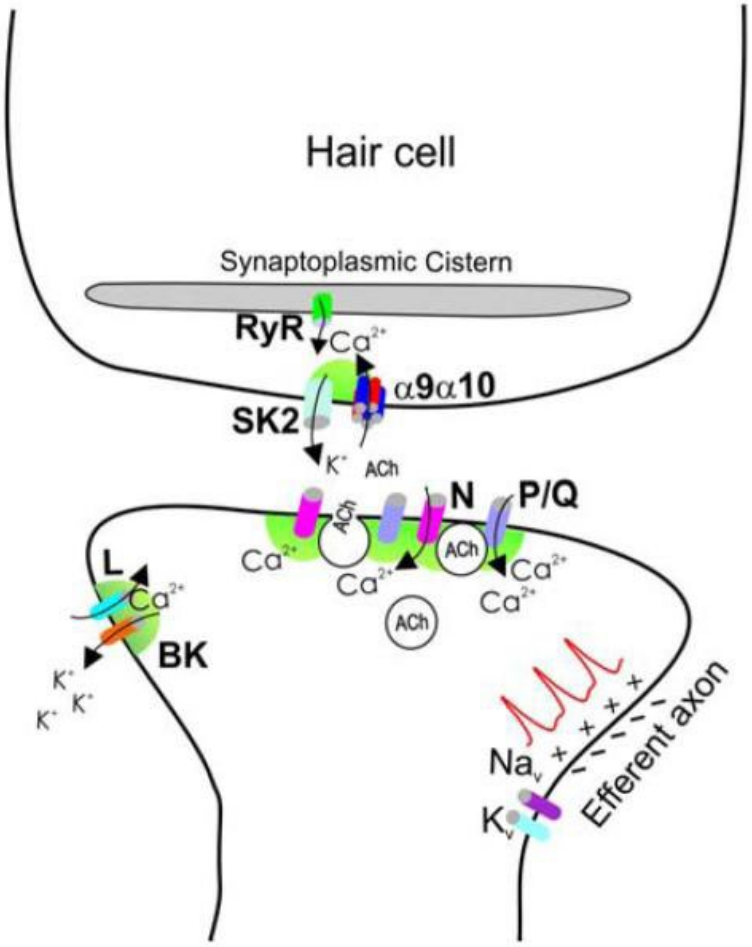

Figure 8: MOC efferent synaptic terminal with relevant proteins and ion movement shown. RyR = Ryanodine Receptor. P/Q, N= different types of VGCCs. L and BK are respectively VGCC and big potassium ion channels, coupled in a manner similar to SK2 and α9α10 nAChR (Elgoyhen and Katz 2012)

Table 1: Summary of MOC efferent reflex

1. High dB SPL sound waves cause the brain to send efferent messages to the cochlea to prevent damage; the exact mechanism of this is not well understood, though it has been proposed that type II afferent synapses on OHCs may play a significant role.
2. Medial Olivocochlear efferent cholinergic fibers innervating the OHC release acetylcholine (ACh) into the synaptic cleft.
3. ACh binds to α9α10 postsynaptic nicotinic acetylcholine receptors (nAChRs) on the basal surface of the OHC.
4. Neurotransmitter binding results in extracellular Ca2+ influx and Ca2+ induced Ca2+ release from synaptoplasic cisternae.
5. Intracellular Ca2+ is bound by calmodulin in the cytosol. The Ca2+, calmodulin complex binds to SK2, opening the channel.
6. This results in K+ efflux, hyperpolarizing the OHC.
7. OHC hyperpolarization causes prestin to relax, elongating the OHC.
8. The OHC lengthens, pushing the basilar membrane away from the tectorial membrane, decreasing the ability of IHC stereocilia to contact the tectorial membrane, and allowing the fluid motion of endolymph to displace the hair cell bundle away from the tallest stereocilia i.e., negative displacement.
9. The result of this system is a reduction of damage caused by high-intensity noise via reduced basilar membrane resonance.

As the OHC is affected by the IPSC, the cell hyperpolarizes, and prestin elongates; this decreases the activation of IHCs by spatially separating them from the tectorial membrane. Additionally, the OHCs have in increase in axial stiffness,

decreasing OHC compliance and further decreasing IHC activation; this is thought to occur because of various secondary messengers and protein kinases which activate in response to MOC efferent activation, though an exact mechanism is yet to be proposed (Dallos et al. 1997). These two mechanisms of sound dampening and increased axial stiffness respectively make up the fast and slow components of OHC sound adaptation via MOC efferent function shown in Figure 9 (Cooper and Guinan 2003).

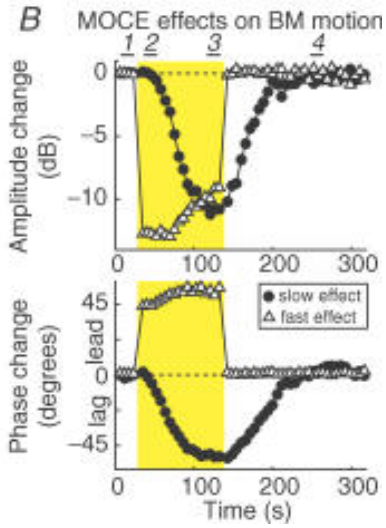

Figure 9: Basilar membrane deflection of fast and slow effects; note the fast effects occur during the noise stimulus (in yellow), and slow effects continue after cessation of stimuli (Cooper and Guinan 2006)

The effector function of the MOC system, in this regard, is to protect IHCs from NIHL. Figure 10 shows that mutant mice lacking functional MOC efferents have worse recoveries from temporary hearing threshold shifts, resulting in long-term hearing loss (Taranda et al. 2009). Mice lacking MOC function have heightened synaptopathy following acoustic exposure compared to WT mice, eventually culminating in HHL (Boero et al. 2018). Additionally, mutant mice with increased MOC function showed an increase in glutamate transmission capabilities (the neurotransmitter used by type I afferents on IHCs) following acoustic exposure, highlighting the importance of the MOC system in hearing transduction (Boero et al. 2018).

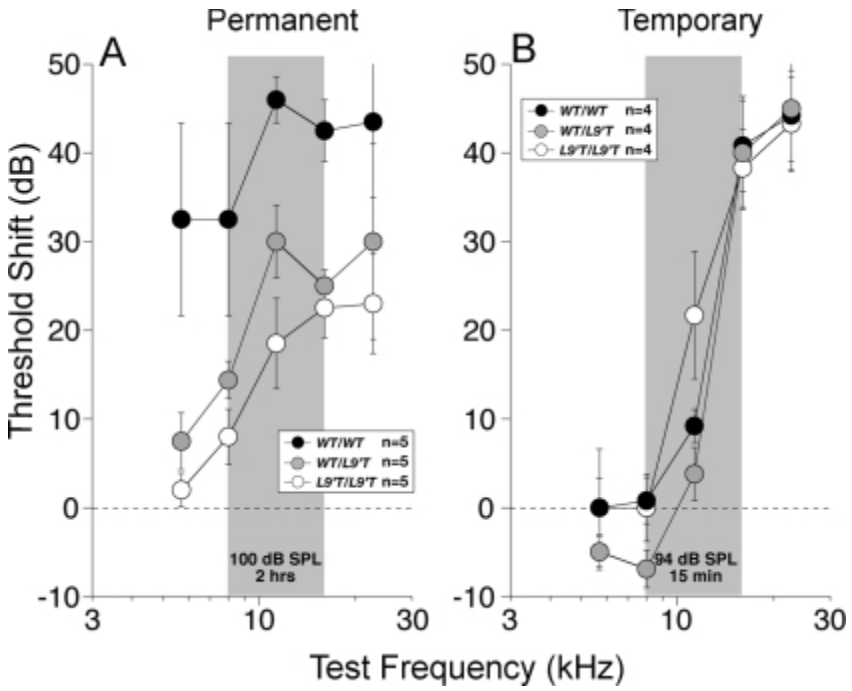

Figure 10: Threshold shifts of WT, heterozygous, and homozygous mice (Chrna9L9'T mutation that enhances MOC activity) shown following 1 week (A) and 6 hours (B) following acoustic exposure of 100 dB noise band. (Taranda et al. 2009)

MOC efferent function primarily reduces the amplitude of basilar membrane motion from sound from low to moderate tones near characteristic frequency. However, it is important to note the presence or absence of background stimuli to the assessed tones. In quiet environments, MOC activation decreases basilar membrane motion and dampens sound acuity. However, in noisy environments, it has been proposed that MOC activation can create an 'antimasking' effect to isolate and amplify a sound within a noisy background, such as picking out a specific instrument in an orchestra (Kawase and Liberman 1993). Evidence of this effect in human populations has not been consistently measure, though human studies of neurectomized patients have shown that the MOC system could play an important role in speech recognition in noise (Zeng et al. 2000).

1.7 Oncomodulin

Oncomodulin (Ocm) is a basolateral EF-hand calcium binding protein (CaBP) similar to alpha-parvalbumin. However, Ocm, also known as beta-parvalbumin, is found in a much narrower range of tissues and as a result appears to provide a more specialized function. Alpha-parvalbumin is found in IHCs, fast twitch muscle fibers, the heart, thymus, lung, kidney, etc., but Ocm is only found in mature OHCs and striolar vestibular hair cells (type 1 and 2), meaning that Ocm is a CaBP specific to the inner ear. Not only do Ocm KO mice show faster onset of hearing loss (as measured by DPOAEs and ABRs), but they also show a faster rate of OHC loss, owing to the importance of Ocm in regulating OHC functionality and survival. It is thought that Ocm acts on OHCs in two ways: first by regulation of Ca2+ transients that effect Rho-dependent actin polymerization and OHC elongation, and second by regulation of Ca2+ transients that are critical for Ca2+/Calmodulin-dependent interactions with prestin. Additionally, Ocm KOs do not show elevated levels of other CaBPs, showing that they cannot be compensated for by upregulating other more generic CaBPs.

CHAPTER TWO

Methods and Materials

2.1 Generation of Ocm KO mice

The Ocm KO mouse model was generated by cloning the 17 kilobase Ocm gene of exons 2-4 on chromosome 5 into a pBluescript KS vector from bacterial DNA. A LoxP site on the 5' end, as well as an Flp-neo-Flp-LoxP cassette on the 3' end was then engineered onto the DNA sequence (Tong et al. 2016). The sequence was then transferred onto embryonic stem cells, of which the clones that underwent homologous recombination were selected for and injected into C57/Bl6 blastocysts. High percentage chimeras were crossed with CBA/CaJ mice to create the KO in an additional genetic background (Tong et al. 2016). Pups were checked for germ-line transmission via Southern blot analysis and PCR genotyping. Cre recombinase allowed for the Ocm gene, now flanked by LoxP, to be knocked out. Ocm KO mice on a C57/Bl6 background how early signs of hearing loss at 1-2 months, and functionally lose their hearing by the 6-month mark (Climer et al. 2021).

This study makes use of *in vivo* data from the genetically modified mice. As such, sample sizes remain small to accommodate the length of time required to generate cochlea from the correct age groups. Additionally, this study primarily serves as a pilot study, showing the technique required to properly stain and count IHC afferent and OHC efferent synapses for comparison.

2.2 Cochlear Microdissection

Adult Ocm KO and WT mice of differing age groups (3-month, 6-month, and 9-month, 1 mouse per group, 6 mice total) on a CBA/CaJ background were generated by Simmons lab and sent to Holt lab, a speech and hearing bioscience and technology lab at Harvard University, for various acoustic (DPOAEs and ABRs) and vestibular testing. Following completion of testing, the mice were sedated, euthanized, and the corresponding inner ears (cochlear and vestibular system) were extracted. Following extraction, the inner ears were sent back to Simmons lab and decalcified in EDTA prior to dissection.

The dissections were performed at a dissecting microscope at room temperature. To start the dissection, the vestibular system and cochlea were separated as the vestibular system will be sectioned, but the cochlea will be further dissected. The cochlea was then bisected, leaving five pieces of the organ of Corti to be removed from the surrounding tissue and stained via immunofluorescence. Figure 11 shows what the organ of Corti looks like prior to being bisected. The organ of Corti must be cut into separate pieces to allow for them to lay flat on a slide, as the natural pitch of the organ of Corti would otherwise prevent this. The tonotopic nature of the cochlea means that different pieces of the organ of Corti correspond to different frequency regions of hearing. As such, the pieces were stained separately to quantify different protein motifs at different frequency regions. Piece 6 and 4 contain the 4 and 22 kHz regions of hearing respectively, while piece 3 and 5 contain the 8 and 32 kHz regions of hearing respectively. The stain protocol thus allows for different high and low frequency protein motifs to be identified.

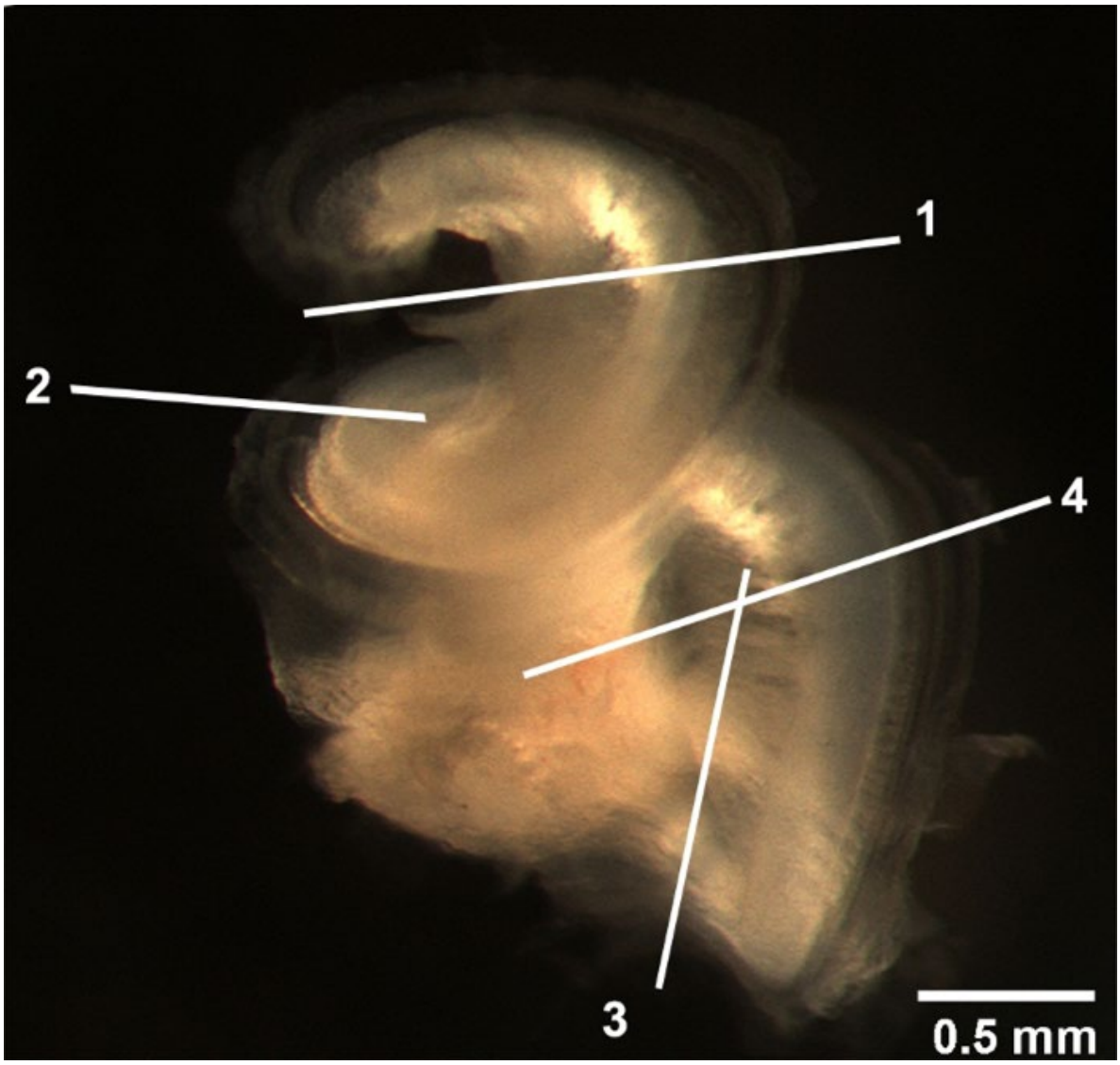

Figure 11: Example cochlea divided into segments corresponding to pieces. The tip near the 1 is the helicotrema, and the other end near the 3 is the location of the oval and round windows (Fang et al. 2019)

2.3 Immunofluorescence

Discussed in this section is the immunofluorescence protocol used for adult mice.

1. Fixation

a. Mice used in this experiment were sacrificed, transcardially perfused with saline, then 4% paraformaldehyde. Cochlea were extracted and put in 1 x phosphate buffered saline (PBS) solution until ready for decalcification.

b. Spirals were dissected in a 35 mL petri dish while immersed in a 1 x PBS solution.

c. Once trimmed into separate pieces, the spirals were transferred to a 1.5 mL centrifuge tube cap. The samples were then each immersed in 150 uL of sucrose solution (30% in PBS) and put on a laboratory shaker plate at 80 rpm at room temperature (20°C) for 30 minutes.

d. Samples were then transferred into a -80°C laboratory freezer for 20 minutes to make the cell membranes brittle.

e. Samples were then transferred into a 37°C laboratory incubator for 30 minutes to crack the frozen membranes, which will help the antibodies stain the sample later.

f. Sucrose solution was then washed off of the samples using PBS. Five total PBS washes were done, two immediately after samples were retrieved from the incubator, and three with 10-minute gaps in between each while the samples sat on a shaker plate.

2. Block

a. The sample was then placed in a 5% normal horse serum solution, diluted in PBS-Triton (NHS-T; 0.3% Triton X-100) for 1 hour on a shaker plate at room temperature. NHS blocks non-specific binding while Triton increases cell permeability, allowing for

antibodies to diffuse into the tissue and bind to the target antigen. Triton additionally decreases the affinity of non-specific antibody binding.

b. The block solution was then changed for the primary antibody solution.

3. Primary antibody administration

a. The primary antibodies were diluted to meet the predetermined antibody working concentrations (Table 2). Antibodies were made in a master mix diluted with 1% NHS.

b. Antibodies were administered to samples in the upside-down tube caps under a dissecting microscope by a micropipette.

c. Following sample immersion in primary antibody solution, the tubes were placed on the caps to limit dehydration. Samples were immersed in 150 µL of solution each.

d. The samples incubated in primary antibody solution overnight in a 37°C incubator to aid in antibody annealing.

4. Secondary antibody administration

a. The samples were removed from the incubator and rinsed eight times in PBS, two immediately, and six with 10-minute gaps between them while they sat on a shaker plate.

b. The secondary antibodies were diluted to meet the predetermined antibody working concentrations (Table 3). Antibodies were made in a master mix diluted with 1% NHS. The total solution volume was 200 µL per sample.

c. Samples were then transferred to the 37°C incubator for 2 hours.

d. Samples were rinsed five times with PBS, two immediately, and three with 10-minute gaps between them while they sat on a shaker plate.

e. Samples stained for CtBP2 and GluR2 had the 'secondary antibody administration' protocol completed twice in succession, starting at step b, to ensure proper staining. After the first round of secondary antibodies were finished incubating, they were removed and a second round of secondaries were applied (same concentration, same incubation time). After this, samples were rinsed and mounted following the normal protocol.

5. Mounting

a. Samples were mounted under a dissecting microscope. A drop of non-hardening VECTASHIELD mounting medium (for fluorescence with 4′,6- diamidino-2-phenylindole (DAPI)) was placed on a clear slide.

b. The sample was placed in the mounting medium, being careful to ensure that the pieces lay with the hair cells facing up. Additionally, the cochlear spiral was made to lay flat on the slide to prevent it from folding over itself.

c. A coverslip was placed over the sample.

d. The coverslip was secured in place by covering its perimeter with nail polish and allowing it to dry.

6. Imaging

a. Imaging was completed using confocal microscopy and Zen software by Zeiss which enabled the user to simultaneously take laser images and analyze them on a nearby desktop. This experiment utilized blue, green, red, and far-red laser channels using the settings shown in Table 4.

b. Z-stacks were taken of the entire area of interest, imaging each focal plane containing protein signals significant of afferent of efferent synapses. After this, the stacks were compressed into a single image for the purpose of counting the synaptic puncta, which was carried out either by hand or via an ImageJ program.

Table 2: Primary Antibody Information

Primary Antibodies				
Antibody Name	Manufacturer	Host	Concentration	Catalog Number
Anti-SK2	Sigma	Rabbit	1:1000	P0483
Anti-ChAT	Millipore	Goat	1:1000	AB144P
Anti-CtBP2	BD Biosciences	Mouse IgG1	1:200	612044
Anti-GluR2	Millipore	Mouse IgG2a	1:200	MAB397

Table 3: Secondary Antibody Information

Secondary Antibodies				
Antibody Name	Manufacturer	Host / Target	Concentration	Catalog Number
Alexa Fluor 647	Life Technologies	Donkey anti Rabbit	1:200	A31573
Alexa Fluor 568	Life Technologies	Donkey anti Goat	1:200	A11057
Alexa Fluor 568	Life Technologies	Goat anti Mouse IgG1	1:200	A21124
Alexa Fluor 488	Life Technologies	Goat anti Mouse IgG2a	1:200	A21131
DAPI	Vector Laboratories, Inc.	NA	NA	NA

2.4 Confocal Microscopy

For quantitative analysis to be completed, all samples had to use the same confocal settings to measure protein presence. The following table (Table 4) shows the relevant confocal settings used in ImageJ for quantitative analysis of particles / presence of synapses.

Table 4: Confocal Laser Settings

Confocal Laser Settings					
Protein Name	Laser Wavelength	Pinhole	Detector Gain	Detector Offset	Detector Digital Gain
CtBP2	561 nm: 1.00%	1.00 AU	700 V	-20	1.0
GluR2	488 nm: 3.50%	1.00 AU	545 V	-20	1.0
ChAT	561 nm: 0.5%	1.00 AU	540 V	-3	1.0
SK2	640 nm: 3.20%	1.00 AU	550 V	-1	1.0

2.5 Image Analysis

Following imaging of samples, the number of OHCs had to be determined, as well as the presence of afferent or efferent synapses at the 22 kHz / 4 kHz, and 32 kHz / 8 kHz regions respectively. The 'Measure Line' plugin for ImageJ, an image processing program developed NIH and LOCI, was used to determine where these frequency regions were on the cochlear pieces. This software calculates the frequencies at different points along the cochlea based on the size of the cochlear pieces. An example of this is shown in Figure 12.

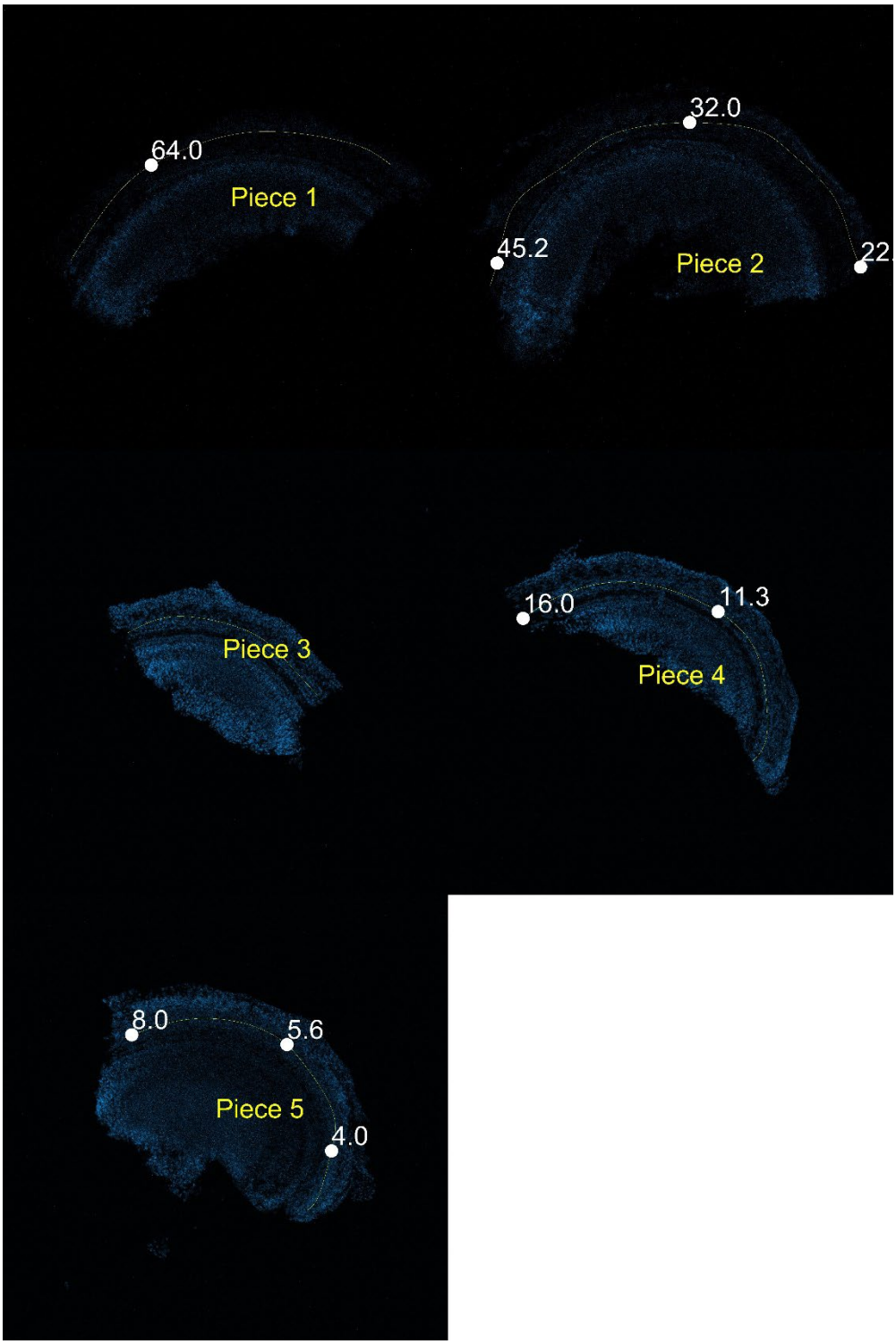

Figure 12: Example frequency map of sample Ocm 342, showing how different frequencies of different pieces is determined and subsequently measured

Images were then taken at these regions for counting. For afferent synapses, 63x magnification images were taken at and around the frequency region for counting. Higher magnification was required for these pieces because CtBP2 and GluR2 will appear to completely overlap at lower magnifications, as opposed to bordering each other at the synaptic cleft. For efferent synapses, 40x magnification images were taken at and around the frequency for counting, as higher magnification was not required. For these 40x images, hair cells and efferent synaptic components were quantified by placed boxes (3 per image) of the following dimensions on the image: W = 54.93 micrometers (704.26 pixels) x H = 37.64 micrometers (482.62 pixels). These dimensions allowed for roughly 10 IHCs per box and aided in the process of counting. Efferent synapses were counted visually by the colocalization of ChAT and SK2 staining on an OHC. For OHC counts, nuclei were counted using the DAPI nuclear stain. OHCs were differentiated from Deiter cells by their elevation, presence of CtBP2, and average size.

The 'Analyze Synapses' plugin was used in ImageJ for counting the number of afferent synapses on IHCs (Dzyubenko et al. 2016). This plugin effectively takes two different channels and combines it into one image that only includes the overlap of both channels, showing the resulting colocalized signal. The Renyi Entropy method for threshold adjustment was used to isolate the CtBP2 and GluR2 signals from background. Additionally, only particles that were between 10 and 400 px^2 were counted, eliminating any noise that artifacts on the image that would be too large or small to be a presynaptic or postsynaptic component.

2.6 Antibody Retrieval

The initial stain of the OHC efferent synapses did not work, and as such the antibodies needed to be retrieved so that the samples could be stained again. A citrate buffer heat-induced retrieval method (HIER-heat-induced epitope retrieval) was used to accomplish this. The samples were placed in a tube cap of sodium citrate buffer and heated to 100°C for 2 hours. It should be noted that the typical antibody retrieval method calls for 20 minutes of heat under pressure, but as a pressure system was not available a longer time was chosen under no pressure. Additionally, the heating apparatus fluctuated between 100°C and 110°C during the retrieval of the Ocm 373 6 mo KO and the Ocm 430 2 mo WT samples. As such, these samples were damaged by the heat, and the corresponding data may be inaccurate. The remaining four samples were heated at 90°C, fluctuating up to 100°C, allowing for proper antibody retrieval while minimizing further damage.

2.7 Statistical Analysis

Quantified values were analyzed using Prism 9 for Windows (version 9.0.0). Unpaired t-tests were used to determine whether groups that differed by genotype or age had statistically significant differences. Standard deviation was also calculated to account for variance. Linear regressions were performed with ‘compare slopes’ function to measure for nonzero slope significance, and to test if the slopes of two different groups were significantly different.

CHAPTER THREE

Results

3.1 Effect of Ocm on OHCs viability at the 4 kHz and 22 kHz regions

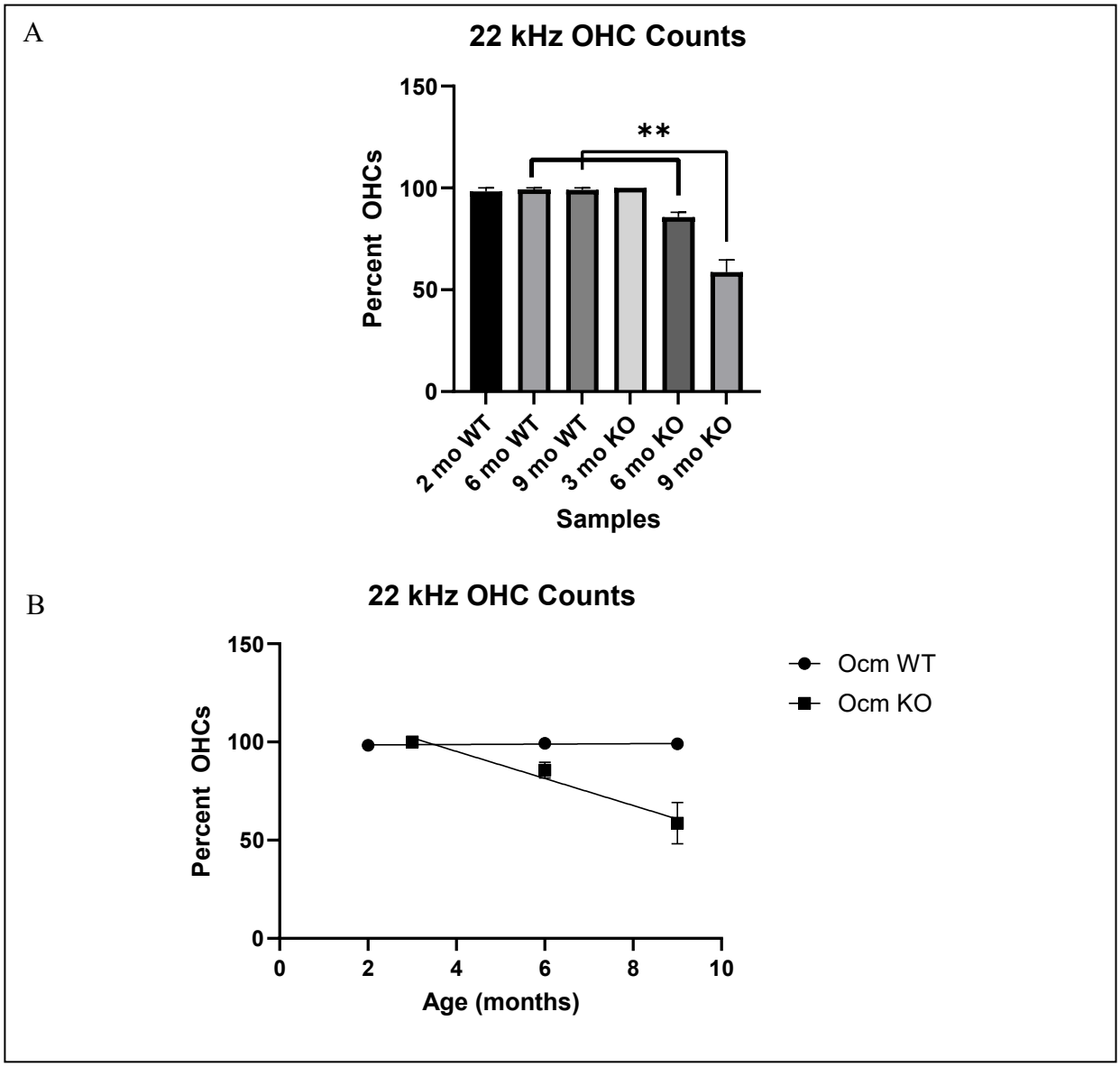

Figure 13: Percent of OHCs present in the 22 kHz region of the Organ of Corti across ages and genotypes counted from DAPI stain. A) OHCs show a decrease in Ocm KOs when compared to WTs. B) Linear regression of data from A. Asterisks (*) indicate a significant difference between WT and KO for the same age ($p < 0.05$, unpaired t-test). n = 3 for each group.

Figure 13 reveals that there is a nonsignificant change in OHC counts in the 22 kHz region in Ocm WT mice as they age from 3 to 9 months. This is in line with the expected values, as it has been shown that CBA WT mice do not typically show a significant change in DPOAE values around the 22 kHz frequency until around 28 months. However, the KO counterparts do show a significant change in OHCs by the 9-month mark, showing an overall decrease in hair cells of about 40 percent. DPOAE studies have shown a significant decrease in OHC function by the 7-month mark in CBA Ocm KOs, therefore this change in OHCs is in line with a decrease in OHC functionality.

When plotted as a linear regression (Figure 13), the slopes of the Ocm WT and KO samples are significantly different ($P < 0.001$). Additionally, the slope of the Ocm KO samples is significantly nonzero ($P < 0.001$), while the slope for the Ocm WT samples is not significantly nonzero ($P < 0.658$).

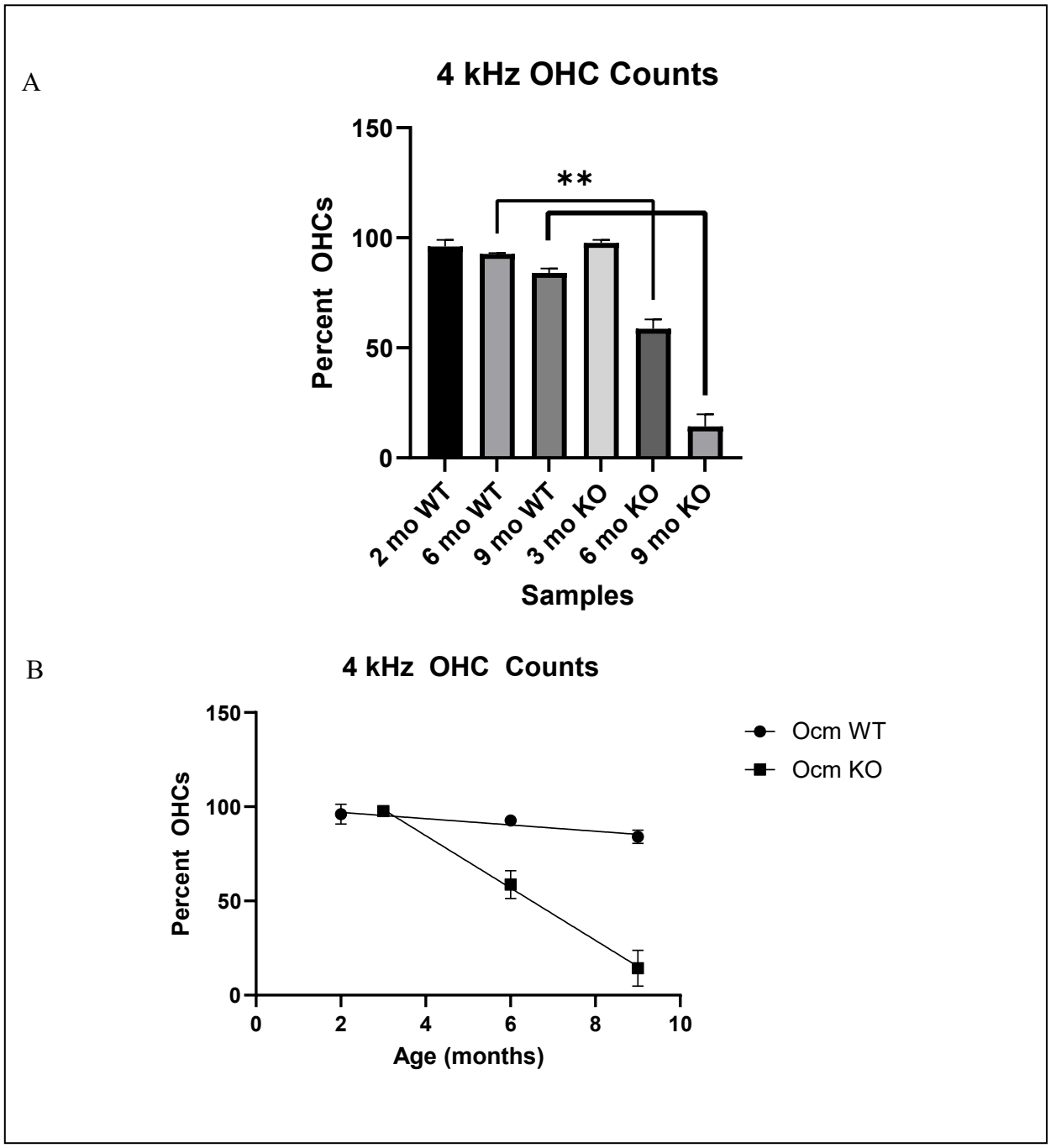

Figure 14: Percent of OHCs present in the 4 kHz region of the Organ of Corti across ages and genotypes counted from DAPI stain. A) OHCs show a decrease in Ocm KOs when compared to WTs. B) Linear regression of data from A. Asterisks (*) indicate a significant difference between WT and KO for the same age ($p < 0.05$, unpaired t-test). $n = 3$ for each group.

Interestingly, at the 4 kHz region, the difference in OHC counts between KOs and WTs is even more exaggerated (Figure 14). Most DPOAE studies have not shown a significant difference between OHC function at the 4 kHz region for Ocm WTs and KOs. Hearing is first lost at high and low frequencies before more medial frequencies- this is because medial frequency hair cells are more densely innervated.

When plotted as a linear regression, the slopes of the Ocm WT and KO samples are significantly different ($P < 0.001$). Additionally, the slope of the Ocm KO samples is significantly nonzero ($P < 0.001$). The slope for the Ocm WT samples is significantly nonzero as well at the 4 kHz region ($P < 0.01$).

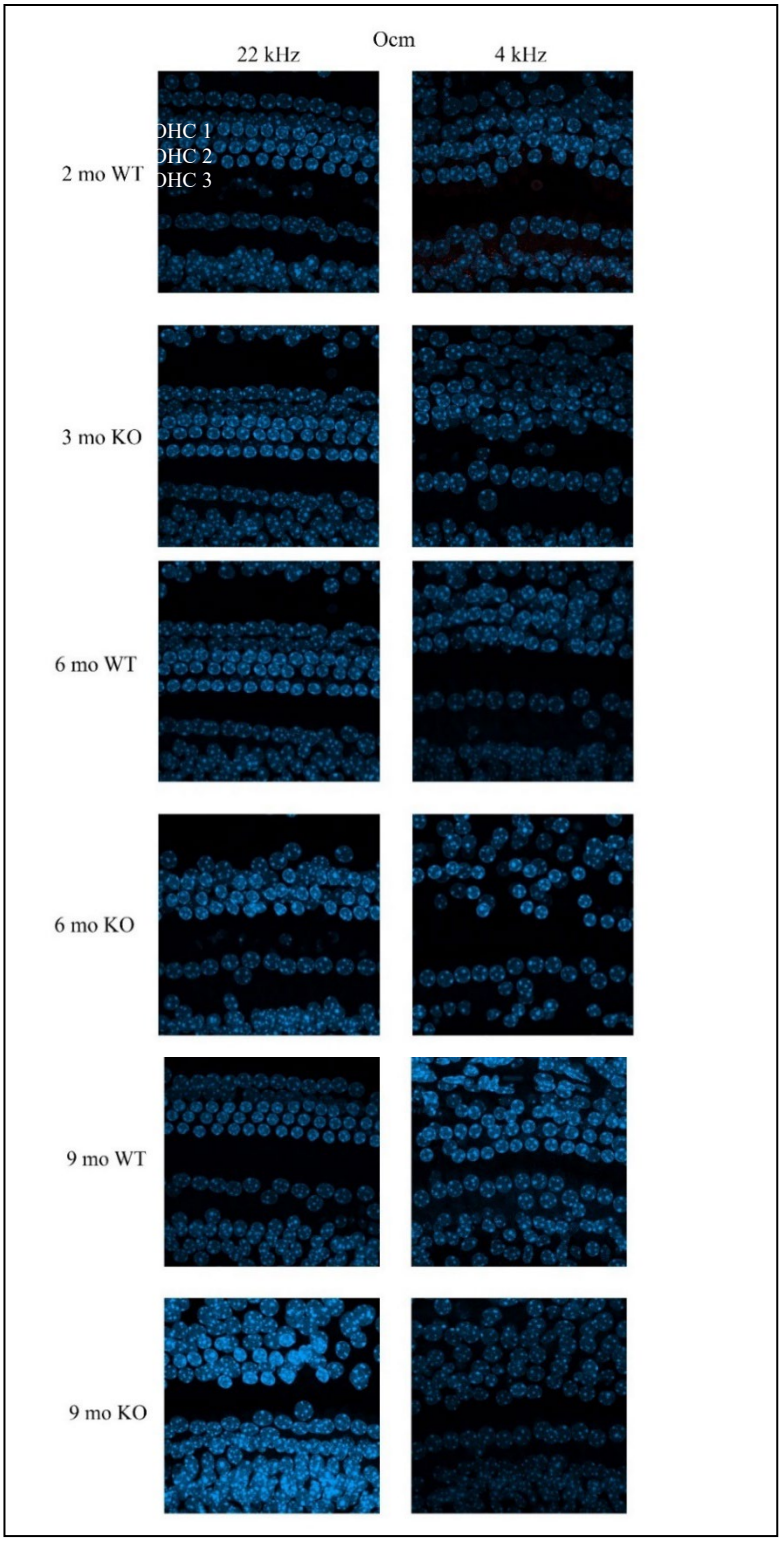

Figure 15: Cochlear pieces stained with DAPI for OHC counts. Immunofluorescence images taken at 63x.

3.2 Effect of Ocm on number of IHC afferent synaptic particles at the 4 kHz and 22 kHz regions

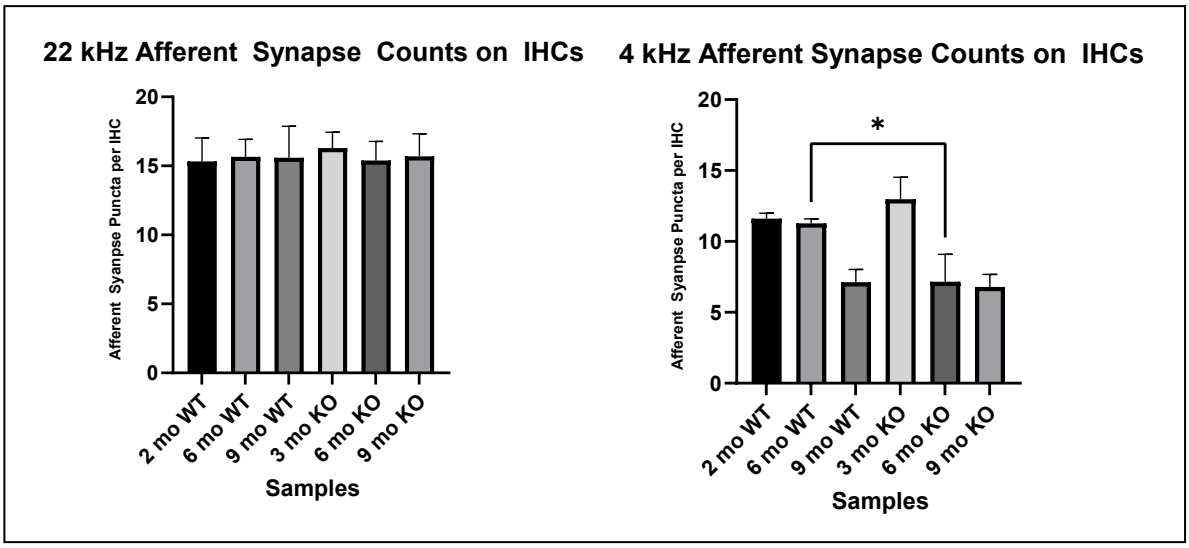

Figure 16: Number of afferent synapses on Ocm KO and WT samples at varying ages. Synaptic counts were carried out by ImageJ plugin 'Synaptic Counts'. Asterisks (*) indicate a significant difference between WT and KO for the same age ($p < 0.05$, unpaired t-test). $n = 3$ for each group.

An afferent synapse was determined when there was colocalization between CtBP2, a presynaptic ribbon at the basal region of OHCs and IHCs, and GluR2, a postsynaptic component that acts as a glutamate receptor, allowing for signal transduction to occur. The 22 kHz region did not show a significant change in number of afferent synapses across ages from 3 months to 9 months of age (Figure 16). At the 4 kHz region, there was a significant difference between the number of afferent synapses between the 6-month Ocm KO and WTs, suggesting that the Ocm KO mice lost their afferent synapses faster than the WT counterparts.

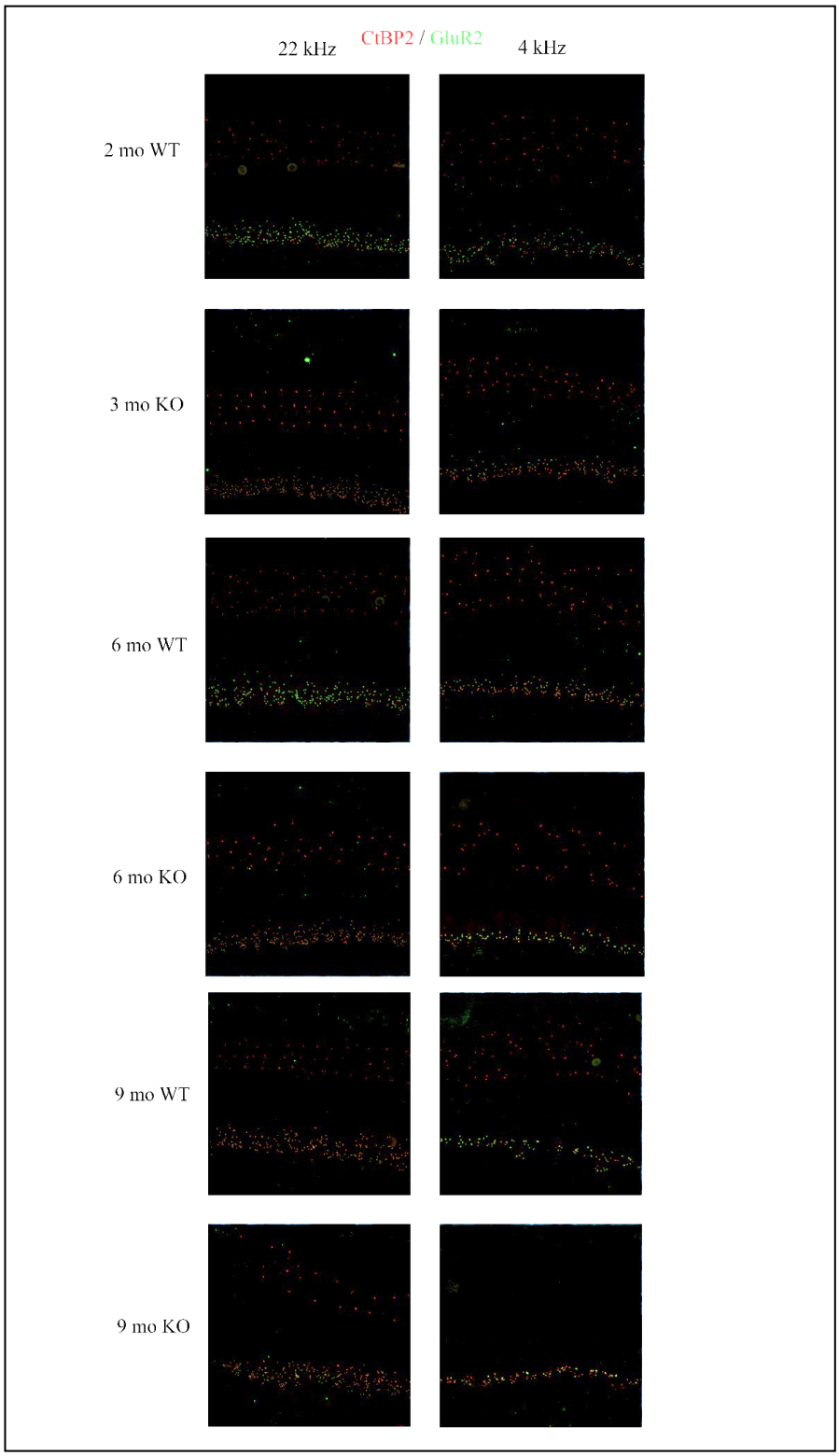

Figure 17: Ocm WT and KO samples shown, stained with CtBP2 on the red channel and GluR2 on the green channel. Immunofluorescence images taken at 63x.

3.3 Effect of Ocm on IHC average afferent synapse size at the 22 kHz and 4 kHz regions

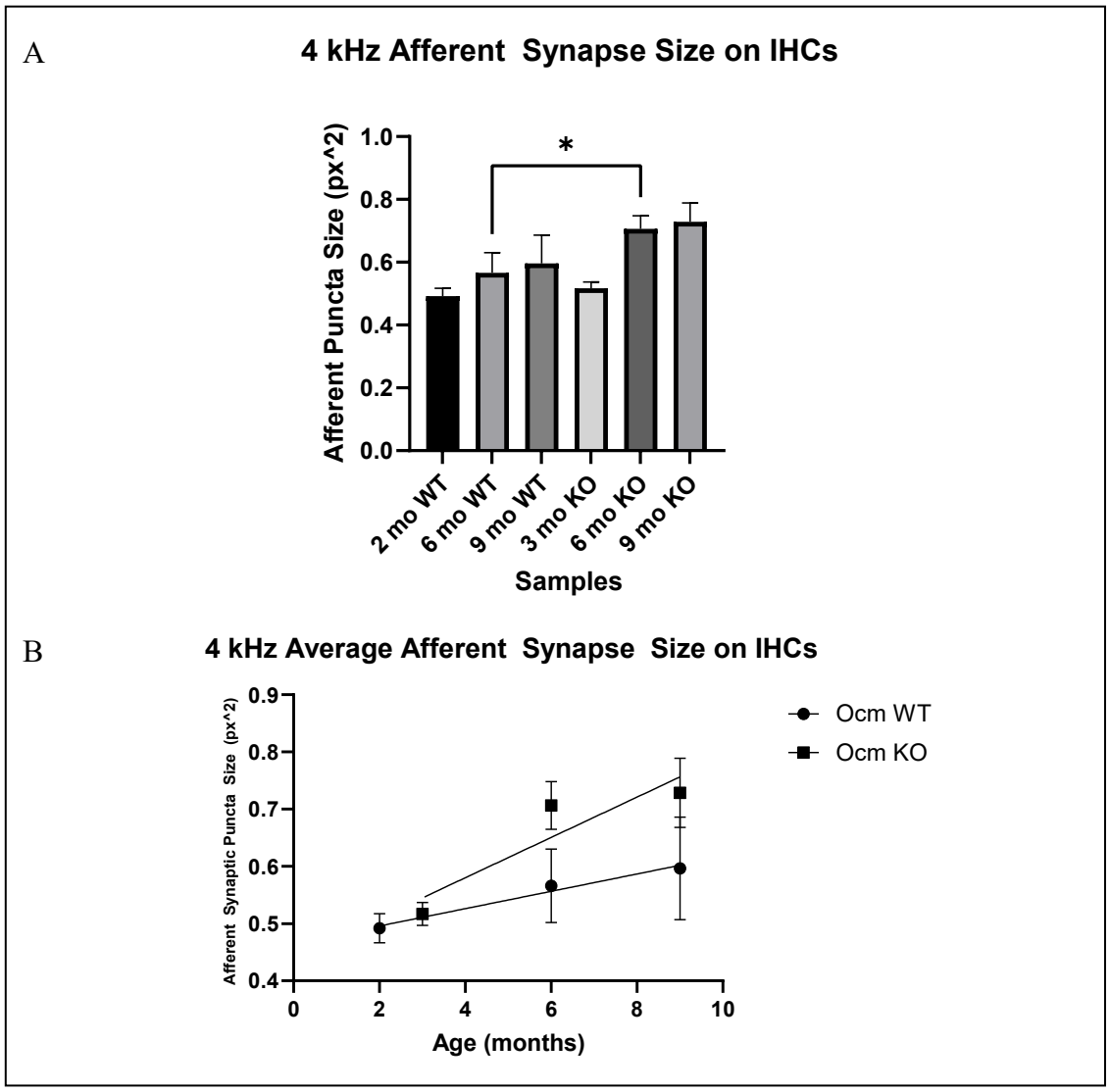

Figure 18: Size of IHC afferent synapses at the 4 kHz region. A) Afferent synaptic size as calculated by 'Analyze Synapses'. B) Linear regression of data from A. Asterisks (*) indicate a significant difference between WT and KO for the same age ($p < 0.05$, unpaired t-test). n = 3 for each group.

The ‘Analyze Synapses’ function also yields the average size of the synaptic particles that it measures. It this case, there was a general upward trend in afferent synapse size as the sample aged in both Ocm WT and KO groups (Figure 18). However, the linear regression shows that the Ocm KO has a significantly nonzero slope ($P < 0.01$), while the Ocm WT group did not ($P > 0.05$).

3.4 Effect of Ocm on OHC counts and OHC Efferent Synapses at the 32 kHz and 8 kHz regions

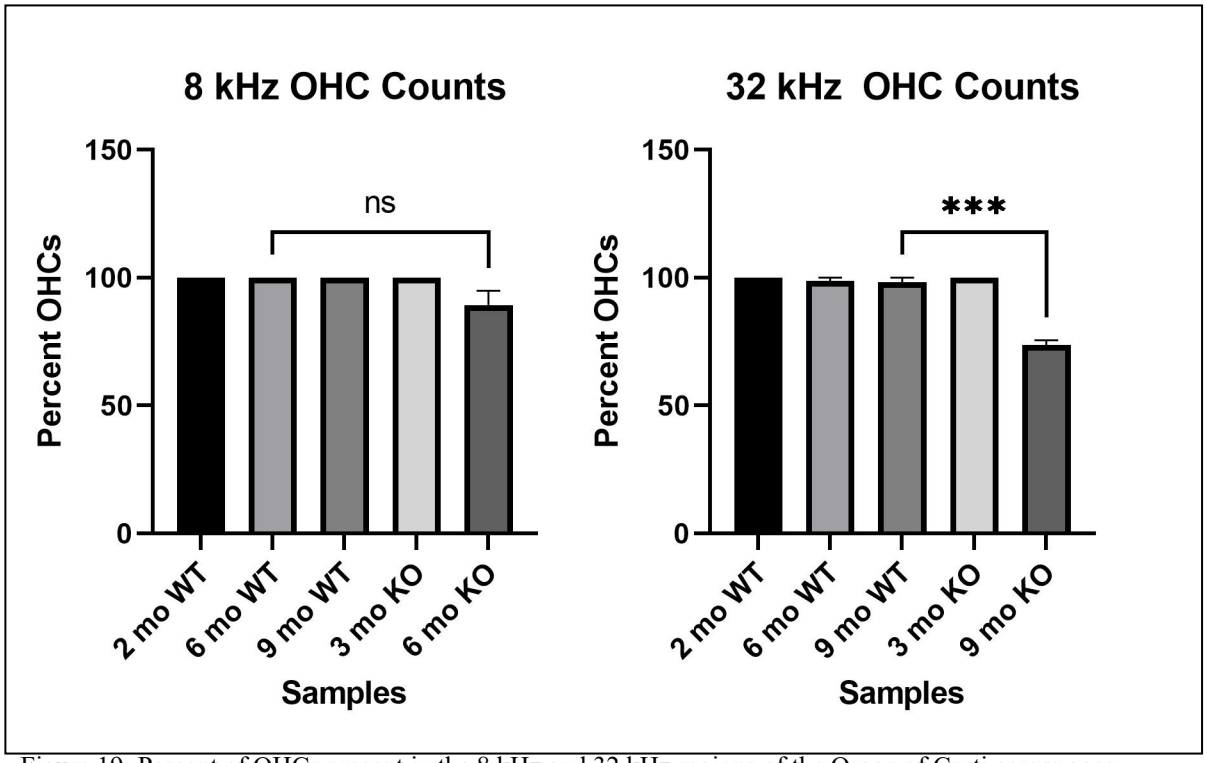

Figure 19: Percent of OHCs present in the 8 kHz and 32 kHz regions of the Organ of Corti across ages and genotypes. Asterisks (*) indicate a significant difference between WT and KO for the same age ($p < 0.05$, unpaired t-test). $n = 3$ for each group.

Ocm appears to have little effect on OHC counts through 6 mo of age (Figure 19). The 8 kHz 9 mo KO sample was damaged during antibody retrieval and subsequently

excluded from the current study. Similarly, the 32 kHz 6 mo KO sample was exluded from the current study for the same reason, though the 32 kHz 9 mo KO allows for a basic trend to still be established. As such, it can be seen that Ocm plays a role in OHC maintanence to the extent that a lack of Ocm results in a loss of OHCs faster than the WT counterparts at the 32 kHz region.

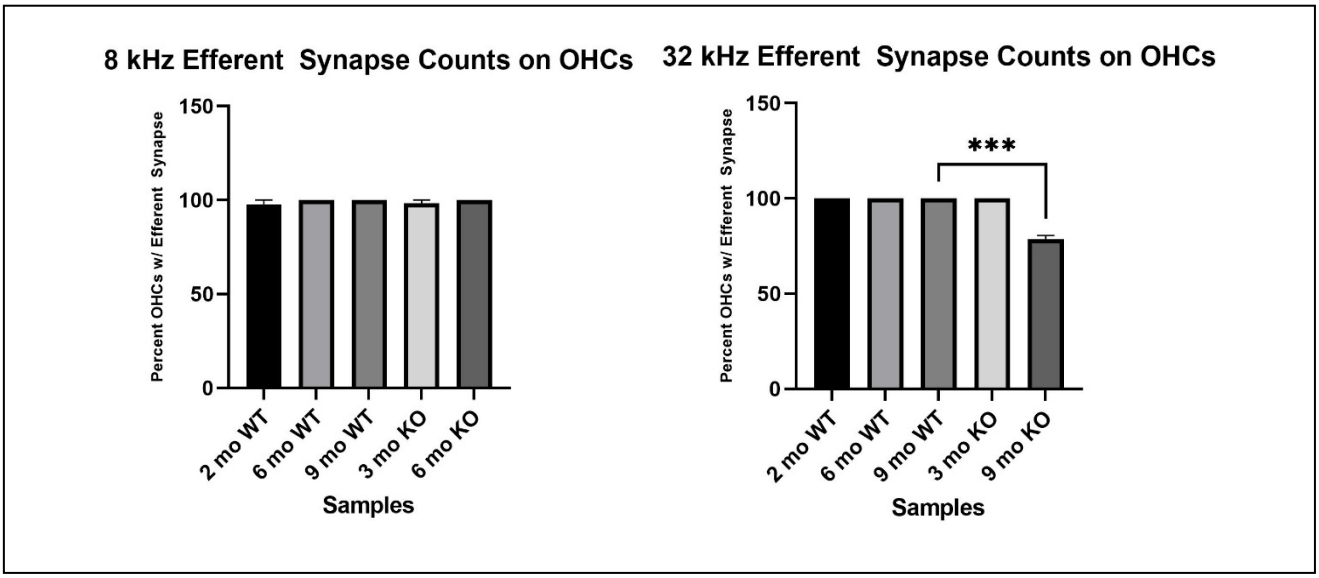

Figure 20: Percent of efferent synapses found in OHCs in the 8 kHz and 32 kHz regions of the Organ of Corti across ages and genotypes. Asterisks (*) indicate a significant difference between WT and KO for the same age ($p < 0.05$, unpaired t-test). n = 3 for each group.

Once again, the lack of data from 2 samples makes comparison across ages difficult. However, there is a significant difference between the number of efferent synapses on the 9 mo WT and 9 mo KO mice (Figure 20). These numbers are a percentage of OHCs with efferent synapses, meaning that there existed some in-tact OHCs without a proper functioning MOC system in the 9 mo KO 32 kHz region.

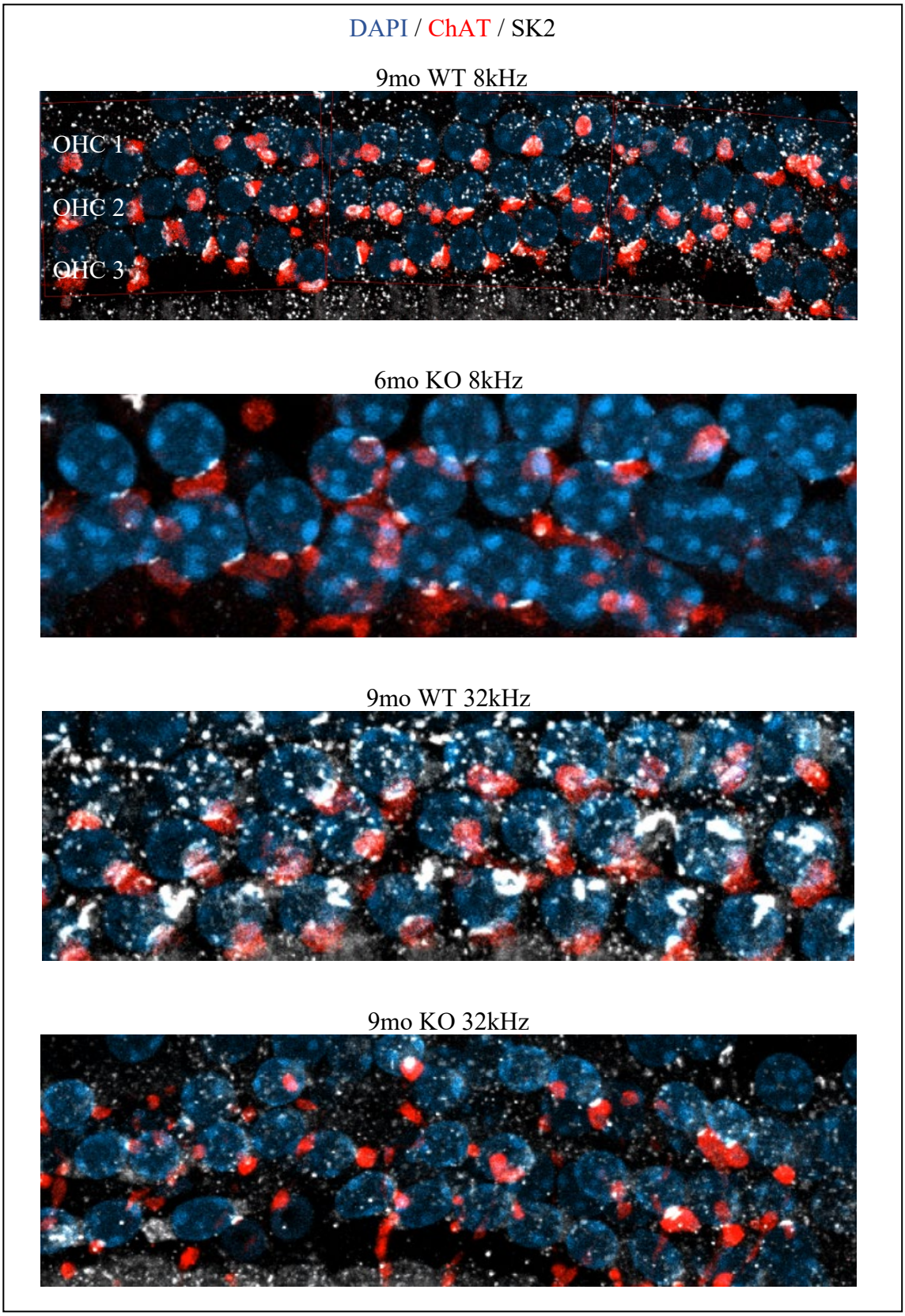

Figure 21: Cochlear pieces from the 8 kHz and 32 kHz regions stained with DAPI on the blue channel, anti-choline acetyltransferase on the red channel, and anti-small potassium channel 2 on the far-red channel (white).

CHAPTER FOUR

Discussion

4.1 OHC counts

When counting the number of OHCs, it quickly became obvious that there was a significant difference between the findings of both Ocm WT and Ocm KO, as well as between the 22 kHz and 4 kHz regions. While two unpaired t-tests show a significant difference between the WT and KO 6 mo and 9 mo samples at the 22 kHz region, perhaps a more interesting finding is the difference between the rates of hair cell loss. When plotted as a linear regression, the KO mice appear to lose OHCs significantly faster than the WT counterparts, which did not show a significantly nonzero slope. For the 4 kHz samples, the WT mice begin to show an apparent trend of OHC loss, however the rate of OHC loss is significantly higher in the KO mice, highlighting the importance of Ocm, and calcium homeostasis generally, in OHC survival. This same trend can be seen in the 8 kHz and 32 kHz regions of OHCs. The 9 mo KO mice showed a significant decrease in OHCs from their WT counterparts at the 32 kHz region, showing an accelerated aging phenotype.

4.2 Afferent synapse counts of IHCs

The 22 kHz IHC afferent synapses showed no significant difference in either the WT or KO mice for all age groups. This is interesting as the number of 22 kHz OHCs of

KO mice was significantly less than the WT mice, indicating that OHC loss precedes loss of hearing function. At the 4 kHz region, while both WT and KO groups showed a negative trend, the 6 mo group had a significant difference between the number of IHC afferent synapses. When plotted as a linear regression, it becomes evident that the 4 kHz KO mice are losing afferent synapses at a faster rate than the WT mice. Importantly, all IHCs still showed some afferent synapses, but the number of synapses was decreasing, showing differing rates of synaptopathy. Interestingly, there appears to be a general inverse correlation between afferent synapse size and number of afferent synapses at the 4 kHz region. This could suggest that as afferent synapses die due to age-related hearing loss, the IHCs create a more robust signal to maintain hearing function. At the 22 kHz region, there was no significant decrease or change in size of afferent synapses.

4.3 Efferent synapse counts of OHCs

While the efferent data is difficult to interpret because of the damaged pieces, resulting in an incomplete comparison between groups, the difference in OHC efferent synapses between 9 mo KO and 9 mo WT mice is very notable. Importantly, the 9 mo KO sample also showed increased OHC degeneration compared to its WT counterpart. The occurrence of some OHCs without an efferent system could suggest that once the efferent system disappears, the OHCs quickly follow. This is supported by the fact that the regions of OHCs with little to no OHC degeneration showed no OHC efferent synapse degeneration, while that of the 9 mo KO, which did show significant, active OHC death also was the only notable region with OHCs missing an MOC efferent

system. This could have large clinical implications for the importance of the efferent system in reducing OHC degeneration, and subsequent hearing loss.

4.4 Future direction and result implications

The present study reveals a significant difference between 9 mo WT and KO OHC counts, but not a significant difference between the 9 mo WT and KO afferent synapse counts in the 4 kHz region, as the only significant difference was between the 6 mo afferent synapse counts. This could potentially mean that the OHCs disappear before the afferent synapses. Additionally, it was shown that the significant OHC loss at the 32 kHz region correlated with a significant decrease in efferent synapse counts. If OHC function is lost before the physical cell dies, then it could be argued that it is the loss of OHC function that leads to eventual presbycusis or NIHL through the loss of this protective mechanism for hearing. The loss of the MOC system not only inhibits the ability of selective hearing, but it also eliminates one of the main protective mechanisms in hearing. The loss of this efferent synapse appears to result in the loss of the OHC, which not only drastically affects hearing thresholds by eliminating the 'cochlear amplifier', but it also exposes IHCs to afferent synaptopathy, causing a direct loss of hearing transduction. If all of this is true, then efferent OHC synapses could be the system that is essential to protect for hearing longevity, and as such could be the target of medical intervention for either preventative measures to decrease the risk of hearing loss, or potential treatments that could encourage efferent synapse regeneration.

Future studies focusing on this should attempt to examine the same frequency regions instead of alternative staining. The same region should be examined with a larger

samples size, allowing for afferent synapse function and degradation to be directly compared to and potentially correlated with efferent synapse function and degradation. Additionally, more data would paint a more complete picture of the trend of afferent and efferent synaptophathy as a function of age, revealing when preventative intervention would prove most vital and most effective.

BIBLIOGRAPHY:

Boero, Luis E., Valeria C. Castagna, Mariano N. Di Guilmi, Juan D. Goutman, Ana Belén Elgoyhen, and María Eugenia Gómez-Casati. 2018. "Enhancement of the Medial Olivocochlear System Prevents Hidden Hearing Loss." *The Journal of Neuroscience* 38 (34): 7440–51. https://doi.org/10.1523/JNEUROSCI.0363-18.2018.

Bosher, S. K., and R. L. Warren. 1968. "Observations on the Electrochemistry of the Cochlear Endolymph of the Rat: A Quantitative Study of Its Electrical Potential and Ionic Composition as Determined by Means of Flame Spectrophotometry." *Proceedings of the Royal Society of London. Series B, Biological Sciences* 171 (1023): 227–47.

Brown, M. C., R. K. de Venecia, and J. J. Guinan. 2003. "Responses of Medial Olivocochlear Neurons. Specifying the Central Pathways of the Medial Olivocochlear Reflex." *Experimental Brain Research* 153 (4): 491–98. https://doi.org/10.1007/s00221-003-1679-y.

Buran, Bradley N., Nicola Strenzke, Andreas Neef, Eckart D. Gundelfinger, Tobias Moser, and M. Charles Liberman. 2010. "Onset Coding Is Degraded in Auditory Nerve Fibers from Mutant Mice Lacking Synaptic Ribbons." *Journal of Neuroscience* 30 (22): 7587–97. https://doi.org/10.1523/JNEUROSCI.0389-10.2010.

Carricondo, Francisco, and Bárbara Romero-Gómez. 2019. "The Cochlear Spiral Ganglion Neurons: The Auditory Portion of the VIII Nerve." *Anatomical Record (Hoboken, N.J.: 2007)* 302 (3): 463–71. https://doi.org/10.1002/ar.23815.

Climer, Leslie K., Aubrey J. Hornak, Kaitlin Murtha, Yang Yang, Andrew M. Cox, Preston L. Simpson, Andy Le, and Dwayne D. Simmons. 2021. "Deletion of Oncomodulin Gives Rise to Early Progressive Cochlear Dysfunction in C57 and CBA Mice." *Frontiers in Aging Neuroscience* 13 (November): 749729. https://doi.org/10.3389/fnagi.2021.749729.

Cooper, N P, and J J Guinan. 2003. "Separate Mechanical Processes Underlie Fast and Slow Effects of Medial Olivocochlear Efferent Activity." *The Journal of Physiology* 548 (Pt 1): 307–12. https://doi.org/10.1113/jphysiol.2003.039081.

———. 2006. "Efferent-Mediated Control of Basilar Membrane Motion." *The Journal of Physiology* 576 (Pt 1): 49–54. https://doi.org/10.1113/jphysiol.2006.114991.

Corns, Laura F., Stuart L. Johnson, Terri Roberts, Kishani M. Ranatunga, Aenea Hendry, Federico Ceriani, Saaid Safieddine, et al. 2018. "Mechanotransduction Is Required for Establishing and Maintaining Mature Inner Hair Cells and Regulating Efferent Innervation." *Nature Communications* 9 (1): 4015. https://doi.org/10.1038/s41467-018-06307-w.

Dallos, P, A. N. Popper, and R. R. Fay. 1996. *The Cochlea*. Vol. 8. Springer New York. https://doi.org/10.1007/978-1-4612-0757-3.

Dallos, Peter, David Z. Z. He, Xi Lin, István Sziklai, Samir Mehta, and Burt N. Evans. 1997. "Acetylcholine, Outer Hair Cell Electromotility, and the Cochlear Amplifier." *The Journal of Neuroscience* 17 (6): 2212–26. https://doi.org/10.1523/JNEUROSCI.17-06-02212.1997.

Dzyubenko, Egor, Andrey Rozenberg, Dirk M. Hermann, and Andreas Faissner. 2016. "Colocalization of Synapse Marker Proteins Evaluated by STED-Microscopy Reveals Patterns of Neuronal Synapse Distribution in Vitro." *Journal of Neuroscience Methods* 273 (November): 149–59. https://doi.org/10.1016/j.jneumeth.2016.09.001.

Elgoyhen, Ana Belén, and Eleonora Katz. 2012. "The Efferent Medial Olivocochlear-Hair Cell Synapse." *Journal of Physiology, Paris* 106 (1–2): 47–56. https://doi.org/10.1016/j.jphysparis.2011.06.001.

Fang, Qiao-Jun, Fan Wu, Renjie Chai, and Su-Hua Sha. 2019. "Cochlear Surface Preparation in the Adult Mouse." *Journal of Visualized Experiments : JoVE*, no. 153 (November): 10.3791/60299. https://doi.org/10.3791/60299.

Fettiplace, Robert. 2017. "Hair Cell Transduction, Tuning and Synaptic Transmission in the Mammalian Cochlea." *Comprehensive Physiology* 7 (4): 1197–1227. https://doi.org/10.1002/cphy.c160049.

Froud, Kristina E., Ann Chi Yan Wong, Jennie M. E. Cederholm, Matthias Klugmann, Shaun L. Sandow, Jean-Pierre Julien, Allen F. Ryan, and Gary D. Housley. 2015. "Type II Spiral Ganglion Afferent Neurons Drive Medial Olivocochlear Reflex Suppression of the Cochlear Amplifier." *Nature Communications* 6 (May): 7115. https://doi.org/10.1038/ncomms8115.

Ghaffari, Roozbeh, Alexander J. Aranyosi, and Dennis M. Freeman. 2007. "Longitudinally Propagating Traveling Waves of the Mammalian Tectorial

Membrane." *Proceedings of the National Academy of Sciences* 104 (42): 16510–15. https://doi.org/10.1073/pnas.0703665104.

Gifford, Margaret L., and John J. Guinan. 1987. "Effects of Electrical Stimulation of Medial Olivocochlear Neurons on Ipsilateral and Contralateral Cochlear Responses." *Hearing Research* 29 (2): 179–94. https://doi.org/10.1016/0378-5955(87)90166-3.

Jing, Zhizi, Mark A. Rutherford, Hideki Takago, Thomas Frank, Anna Fejtova, Darina Khimich, Tobias Moser, and Nicola Strenzke. 2013. "Disruption of the Presynaptic Cytomatrix Protein Bassoon Degrades Ribbon Anchorage, Multiquantal Release, and Sound Encoding at the Hair Cell Afferent Synapse." *Journal of Neuroscience* 33 (10): 4456–67. https://doi.org/10.1523/JNEUROSCI.3491-12.2013.

Johnson, Stuart L., and Walter Marcotti. 2008. "Biophysical Properties of CaV1.3 Calcium Channels in Gerbil Inner Hair Cells." *The Journal of Physiology* 586 (4): 1029–42. https://doi.org/10.1113/jphysiol.2007.145219.

Kawase, T., and M. C. Liberman. 1993. "Antimasking Effects of the Olivocochlear Reflex. I. Enhancement of Compound Action Potentials to Masked Tones." *Journal of Neurophysiology* 70 (6): 2519–32. https://doi.org/10.1152/jn.1993.70.6.2519.

Kujawa, Sharon G., and M. Charles Liberman. 2009. "Adding Insult to Injury: Cochlear Nerve Degeneration after 'Temporary' Noise-Induced Hearing Loss." *The Journal of Neuroscience* 29 (45): 14077–85. https://doi.org/10.1523/JNEUROSCI.2845-09.2009.

Liberman, M. C., and M. C. Brown. 1986. "Physiology and Anatomy of Single Olivocochlear Neurons in the Cat." *Hearing Research* 24 (1): 17–36. https://doi.org/10.1016/0378-5955(86)90003-1.

Liberman, M. Charles, Jiangang Gao, David Z. Z. He, Xudong Wu, Shuping Jia, and Jian Zuo. 2002. "Prestin Is Required for Electromotility of the Outer Hair Cell and for the Cochlear Amplifier." *Nature* 419 (6904): 300–304. https://doi.org/10.1038/nature01059.

Lioudyno, M. 2004. "A 'Synaptoplasmic Cistern' Mediates Rapid Inhibition of Cochlear Hair Cells." *Journal of Neuroscience* 24 (49): 11160–64. https://doi.org/10.1523/JNEUROSCI.3674-04.2004.

Liu, Yi-Wen, and Stephen T. Neely. 2009. “Outer Hair Cell Electromechanical Properties in a Nonlinear Piezoelectric Model.” *The Journal of the Acoustical Society of America* 126 (2): 751–61. https://doi.org/10.1121/1.3158919.

Lopez-Poveda, Enrique A. 2018. “Olivocochlear Efferents in Animals and Humans: From Anatomy to Clinical Relevance.” *Frontiers in Neurology* 9 (March): 197. https://doi.org/10.3389/fneur.2018.00197.

Maison, Stéphane F., Xiao-Ping Liu, Ruth Anne Eatock, David R. Sibley, David K. Grandy, and M. Charles Liberman. 2012. “Dopaminergic Signaling in the Cochlea: Receptor Expression Patterns and Deletion Phenotypes.” *The Journal of Neuroscience: The Official Journal of the Society for Neuroscience* 32 (1): 344–55. https://doi.org/10.1523/JNEUROSCI.4720-11.2012.

Maison, Stéphane, Leslie D. Liberman, and M. Charles Liberman. 2016. “Type II Cochlear Ganglion Neurons Do Not Drive the Olivocochlear Reflex: Re-Examination of the Cochlear Phenotype in Peripherin Knock-Out Mice.” *ENeuro* 3 (4): ENEURO.0207-16.2016. https://doi.org/10.1523/ENEURO.0207-16.2016.

Martini, Frederic. 1998. “Fundamentals of Anatomy and Physiology.” In . Prentice Hall.

Müller, Marcus, Karen von Hünerbein, Silvi Hoidis, and Jean W. T. Smolders. 2005. “A Physiological Place–Frequency Map of the Cochlea in the CBA/J Mouse.” *Hearing Research* 202 (1): 63–73. https://doi.org/10.1016/j.heares.2004.08.011.

Nadol, J. B., M. J. Mulroy, D. A. Goodenough, and T. F. Weiss. 1976. “Tight and Gap Junctions in a Vertebrate Inner Ear.” *The American Journal of Anatomy* 147 (3): 281–301. https://doi.org/10.1002/aja.1001470304.

Pickles, James. 1988. “An Introduction to the Physiology of Hearing (2nd Ed).” *Academic Press*.

Pollock, Lana M., and Brian M. McDermott Jr. 2015. “The Cuticular Plate: A Riddle, Wrapped in a Mystery, inside a Hair Cell.” *Birth Defects Research Part C: Embryo Today: Reviews* 105 (2): 126–39. https://doi.org/10.1002/bdrc.21098.

Qiu, Xufeng, and Ulrich Müller. 2018. “Mechanically Gated Ion Channels in Mammalian Hair Cells.” *Frontiers in Cellular Neuroscience* 12 (April): 100. https://doi.org/10.3389/fncel.2018.00100.

Rasmussen. 1946. “The Olivary Peduncle and Other Fiber Projections of the Superior Olivary Complex.” Journal of Comparative Neurology - Wiley Online Library. 1946. https://onlinelibrary.wiley.com/doi/abs/10.1002/cne.900840204?sid=nlm%3Apubmed.

Taranda, Julian, Stéphane F Maison, Jimena A Ballestero, Eleonora Katz, Jessica Savino, Douglas E Vetter, Jim Boulter, M. Charles Liberman, Paul A Fuchs, and A. Belén Elgoyhen. 2009. “A Point Mutation in the Hair Cell Nicotinic Cholinergic Receptor Prolongs Cochlear Inhibition and Enhances Noise Protection.” *PLoS Biology* 7 (1): e1000018. https://doi.org/10.1371/journal.pbio.1000018.

Tong, Benton, Aubrey J. Hornak, Stéphane F. Maison, Kevin K. Ohlemiller, M. Charles Liberman, and Dwayne D. Simmons. 2016. “Oncomodulin, an EF-Hand Ca2+ Buffer, Is Critical for Maintaining Cochlear Function in Mice.” *The Journal of Neuroscience* 36 (5): 1631–35. https://doi.org/10.1523/JNEUROSCI.3311-15.2016.

Warr, W. Bruce, and John J. Guinan. 1979. “Efferent Innervation of the Organ of Corti: Two Separate Systems.” *Brain Research* 173 (1): 152–55. https://doi.org/10.1016/0006-8993(79)91104-1.

Zeng, Fan-Gang, Kristina M. Martino, Fred H. Linthicum, and Sigfrid D. Soli. 2000. “Auditory Perception in Vestibular Neurectomy Subjects.” *Hearing Research* 142 (1): 102–12. https://doi.org/10.1016/S0378-5955(00)00011-3.